

Renata Ligocki Pedro

**Optimization of Steel-Concrete Composite  
I-Girder Bridges**

Brazil  
2017



Renata Ligocki Pedro

# **Optimization of Steel-Concrete Composite I-Girder Bridges**

Master's Thesis presented as a partial requirement for obtaining a Master's degree in Civil Engineering from the Federal University of Santa Catarina

Federal University of Santa Catarina  
Department of Civil Engineering  
Graduation program in Civil Engineering  
Advisor: Prof. Leandro Fleck Fadel Miguel  
Co-advisor: Prof. Rafael Holdorf Lopez

Brazil  
2017



Ficha de identificação da obra elaborada pelo autor,  
através do Programa de Geração Automática da Biblioteca Universitária da UFSC.

Ligocki Pedro, Renata  
Optimization of Steel-Concrete Composite I  
Girder Bridges / Renata Ligocki Pedro ; orientador,  
Leandro Fleck Fadel Miguel, coorientador, Rafael  
Holdorf Lopez, 2017.  
135 p.

Dissertação (mestrado) - Universidade Federal de  
Santa Catarina, Centro Tecnológico, Programa de Pós  
Graduação em Engenharia Civil, Florianópolis, 2017.

Inclui referências.

1. Engenharia Civil. 2. Estrutura Mista. 3.  
Ponte. 4. Otimização. 5. Método dos Elementos  
Finitos. I. Fleck Fadel Miguel, Leandro. II.  
Holdorf Lopez, Rafael. III. Universidade Federal de  
Santa Catarina. Programa de Pós-Graduação em  
Engenharia Civil. IV. Título.

Renata Ligocki Pedro

## **Optimization of Steel-Concrete Composite I-Girder Bridges**

Esta Dissertação foi julgada adequada para obtenção do Título de "Mestre", e aprovada em sua forma final pelo Programa de Pós-graduação em Engenharia Civil

Florianópolis, 29 de Maio de 2017:

---

Prof. Dr. Glicério Trichês  
Coordenador do Curso

---

Prof. Dr. Leandro Fleck Fadel Miguel  
Orientador

---

Prof. Dr. Rafael Holdorf Lopez  
Co-Orientador  
Banca Examinadora:

---

Prof. Roberto Caldas de Andrade Pinto, PhD.  
Universidade Federal de Santa Catarina

---

Prof. Dr. José Carlos de Carvalho Pereira  
Universidade Federal de Santa Catarina

---

Prof. Dr. Ricardo Hallal Fakury  
Universidade Federal de Minas Gerais  
(vídeo-conferência)





# Acknowledgments

This work was carried out during the years 2015-2017 at the Civil Engineering Department, Federal University of Santa Catarina. It is a pleasure to thank those who made this dissertation possible.

First, I am forever indebted to my parents, for their support throughout my entire life. Without them I couldn't have achieved any of my dreams. My warmest gratitude also goes to my sister, who shared her experience and let me learn through her difficulties.

I am deeply grateful to my advisor Professor Leandro Fleck Fadel Miguel. Without his continuous enthusiasm and encouragement this study couldn't have reached its completion. Also, I'd like to thank my co-advisor, Professor Rafael Holdorf Lopez, who shared his knowledge about optimization tools and turned this study possible.

I want to express my gratitude to the other contributors of this thesis: Professor Daniel Loriggio, for teaching me even more about bridges structural behavior; Professors Ricardo Hallal Fakury, José Carlos de Carvalho Pereira and Roberto Caldas de Andrade Pinto, for sharing their knowledge and improving this work.

I also owe a great debt of gratitude to Professor Cláudio Cezar Zimmerman and the PET group, for helping me start in the engineering universe, navigating with me through all the different fields, learning together, and making me the person and professional that I am today.

I cannot forget to thank my colleagues: Juliano Demarche, for sharing his knowledge in Finite Element Models, facilitating my learning in the matter; Rafael Souza, for always being prompt to help me in anything that I needed.



*“We build too many walls and not enough bridges.”*

Isaac Newton



# Abstract

This work presents an efficient two-stage optimization approach to the design of steel-concrete composite I-girder bridges. In the first step, a simplified structural model, usually adopted by bridge designers, is employed aiming to locate the global optimum region and provide a starting point to the local search. Then, a finite element model (FEM) is used to refine and improve the optimization. Through this procedure, it is possible to combine the low computational cost required on the first stage with the accuracy provided on the second one. For illustration purposes, a numerical example of a composite bridge designed by Pinho & Bellei (2007) and studied by Leitão et al. (2011) is assessed. The objective function is based on the economic cost of the structure. Due to the non-convex nature of the problem and to the presence of discrete variables, the first stage optimization is conducted through five well-known meta-heuristic algorithms: Backtracking Search Algorithm (BSA), Firefly Algorithm (FA), Genetic Algorithm (GA), Imperialist Competitive Algorithm (ICA) and Search Group Algorithm (SGA). The SGA is chosen to pursue the second stage because a statistical analysis has demonstrated that it achieved the best performance. It is shown that the proposed scheme is able to reduce the structural cost in up to 7.43% already in the first stage and can reach up to 9.17% of saving costs in the end of the optimization procedure.

**Key-words:** Composite Structure. Bridge. Optimization. Finite Element Method.



# Resumo Expandido

Pontes são estruturas importantes para travessia de rios e vales. Elas começaram a ser construídas em 62 a.C. em Roma, usando a técnica de arcos de pedra. Com o passar do tempo, as técnicas e os materiais empregados em pontes foram evoluindo, de arco em pedra para madeira treliçada, chegando até a tecnologia de pontes pênseis e estaiadas. As pontes mistas de aço e concreto surgiram em 1930, com a laje de concreto armado e as vigas em seção I ou caixa.

As pontes mistas de seção I são muito econômicas para estruturas retas com vãos pequenos (20 a 50m). Essa estrutura tem sua importância comprovada pela quantidade de trabalhos na área. - Madrazo-Aguirre, Ruiz-Teran & Wadee (2015), Liu et al. (2014), Zhou et al. (2016), Liu et al. (2009), Ellobody (2014), Oehlers (1990), Gocál & Ďuršová (2012), Pinho & Bellei (2007), Fernandes (2008), Klinsky (1999), Leitão et al. (2011), Vitória (2015) e Fabeane (2015). Porém, nenhum desses estudos focam na otimização completa da estrutura.

Na área de otimização de pontes, há também um grande número de trabalhos na literatura. Alguns autores optaram por otimizar os cabos de pontes estaiadas - Lute, Upadhyay & Singh (2009), Cai & Aref (2015), Martins, Simões & Negrão (2015), Baldomir et al. (2010) e Hassan (2013). Outros estudaram a otimização de pontes de grandes vãos - Kusano et al. (2014) -, pontes de treliça metálica - Cheng (2010) e Cheng, Qian & Sun (2013) -, pontes de concreto protendido - Martí et al. (2013) e Kaveh, Maniat & Naeni (2016) - e pontes de pilares altos - Martínez et al. (2011). Na otimização de pontes mistas, pode-se citar o trabalho de Gocál & Ďuršová (2012), que realizou um estudo paramétrico para otimizar a disposição transversal das vigas. Logo, é importante reiterar que não foi encontrado nenhum trabalho de otimização da estrutura completa de pontes mistas. Além disso, a importância do tema é também contabilizada na separação entre a eficiência do projeto e a experiência

do projetista. Baseado na otimização de outras estruturas, espera-se obter uma redução de até 10% do custo da ponte.

Assim, o principal objetivo desta dissertação é otimizar o projeto de pontes mistas de aço e concreto. Para isso, é proposta uma metodologia de otimização dividida em dois estágios. Na primeira etapa, um modelo estrutural simplificado, usualmente adotado por projetistas, é utilizado para achar a região ótima, assim como para indicar um ponto inicial para a busca seguinte. No segundo estágio, um modelo de elementos finitos utilizando barras e cascas é incorporado para melhorar a otimização. Essa estratégia é empregada para combinar o benefício de cada estágio na resolução desse problema. Enquanto que o primeiro estágio tem um custo computacional baixo, podendo ser repetido inúmeras vezes, a segunda etapa é mais precisa estruturalmente. Logo, com a combinação dos dois modelos, o projeto pode ser otimizado de forma precisa com um tempo computacional razoável.

Ainda, para resolver esse problema, é preciso definir o método de otimização. Por causa da complexidade do problema e da presença de variáveis discretas, optou-se por utilizar algoritmos heurísticos. Como não existe um algoritmo universal, foram testados estatisticamente cinco algoritmos heurísticos conhecidos: *Backtracking Search Algorithm* (BSA), *Firefly Algorithm* (FA), *Genetic Algorithm* (GA), *Imperialist Competitive Algorithm* (ICA) e *Search Group Algorithm* (SGA). Dentre eles, o SGA foi o que teve a melhor performance para resolver essa otimização.

Com a escolha do SGA, a otimização em duas etapas foi realizada. Foi, então, otimizada uma ponte mista bi-apoiada com 40m de vão livre e 13m de largura. Na primeira etapa, atingiu-se um custo de U\$119.796,43 e na segunda, U\$117.884,93. Comparando esses resultados com uma ponte de mesmas características projetada manualmente por Pinho &



Bellei (2007), alcançou-se uma redução de 9,17%.

Os resultados alcançados mostram que a metodologia proposta é eficiente na redução de custo da ponte. Outros estudos devem ser efetuados, tais como o da influência da passagem dinâmica de veículos, para aumentar a confiança estrutural.

**Palavras-chave:** Estrutura Mista. Ponte. Otimização. Método dos Elementos Finitos.



# List of Figures

Figure 1 – Fabricio bridge, Rome - Italy . . . . .	36
Figure 2 – Pedro Ivo Campos bridge, Florianópolis - Brazil . . .	36
Figure 3 – Perimetral viaduct, Rio de Janeiro - Brazil . . . . .	37
Figure 4 – Steel-concrete composite I-girder bridge . . . . .	47
Figure 5 – Parts of a steel-concrete composite I-girder bridge . .	48
Figure 6 – Vehicle TB-45 . . . . .	49
Figure 7 – Level rule for the tire load . . . . .	59
Figure 8 – Level rule for the uniform loading . . . . .	59
Figure 9 – Fauchart Model . . . . .	60
Figure 10 – Beam element . . . . .	62
Figure 11 – Eccentricity between slab and beam axis . . . . .	64
Figure 12 – Quadrilateral element of the Serendipity family . . .	67
Figure 13 – Quadrilateral element of the Serendipity family by the Mindlin theory . . . . .	69
Figure 14 – Local and global minimum . . . . .	75
Figure 15 – BSA flowchart . . . . .	77
Figure 16 – FA flowchart . . . . .	79
Figure 17 – GA flowchart . . . . .	81
Figure 18 – ICA flowchart . . . . .	83
Figure 19 – SGA flowchart . . . . .	85
Figure 20 – Statistic Tests . . . . .	87
Figure 21 – Bridge cross-section . . . . .	90
Figure 22 – Beam geometric design variables . . . . .	91
Figure 23 – Bridge top view . . . . .	91
Figure 24 – Beam accessories . . . . .	91
Figure 25 – Composite Section . . . . .	92
Figure 26 – Optimization procedure flowchart . . . . .	97
Figure 27 – Cross-section of the bridge studied in Pinho & Bellei (2007) and Leitão et al. (2011) . . . . .	100

Figure 28 – SAP2000 model . . . . .	101
Figure 29 – Stress distribution . . . . .	104
Figure 30 – Stress distribution (zoom) . . . . .	104
Figure 31 – Convergence history comparison of all the algorithms used . . . . .	106
Figure 32 – Results of the ANOVA test for 200,000 OFEs . . . . .	107
Figure 33 – Comparison of the means of the algorithms . . . . .	108
Figure 34 – Convergence history of the two-stage based optimization	111
Figure 35 – Rüsç’s table 14 . . . . .	132
Figure 36 – Rüsç’s table 27 . . . . .	133
Figure 37 – Rüsç’s table 98 - part 1 . . . . .	134
Figure 38 – Rüsç’s table 98 - part 2 . . . . .	135

# List of Tables

Table 1 – Statistic Tests . . . . .	87
Table 2 – Prices . . . . .	94
Table 3 – Bounds of the variables . . . . .	101
Table 4 – Results . . . . .	103
Table 5 – Comparison of internal forces . . . . .	103
Table 6 – Algorithms Parameters . . . . .	105
Table 7 – Results for 200,000 OFEs . . . . .	105
Table 8 – Results of the ANOVA test for 200,000 OFEs . . . . .	107
Table 9 – Comparison of design solutions with 4 beams - Allowable Stresses . . . . .	110
Table 10 – Comparison of costs . . . . .	110
Table 11 – Comparison of internal forces . . . . .	110
Table 12 – Comparison of design solutions using Fauchart - Allowable Stresses . . . . .	112
Table 13 – Comparison of internal forces . . . . .	112
Table 14 – LRFD design using Level Rule Model on first stage . . . . .	113
Table 15 – LRFD design using Fauchart Model on first stage . . . . .	114
Table 16 – Comparison of internal forces . . . . .	114
Table 17 – Comparison of internal forces . . . . .	115



# List of abbreviations and acronyms

AASHTO	American Association of State Highway and Transportation Officials
ABNT	Brazilian Association of Technical Standards
ACO	Ant Colony Optimization
ANOVA	Analysis of Variance
BSA	Backtracking Search Algorithm
CBO	Colliding Bodies Optimization
CFRP	Carbon Fiber Reinforced Polymeric
DOF	Degrees of Freedom
FA	Firefly Algorithm
FEM	Finite Element Model
FM	Fauchart Model
GA	Genetic Algorithm
IBGE	Brazilian Institute of Statistics and Geography
ICA	Imperialist Competitive Algorithm
LR	Level Rule
NBR	Brazilian Standard
OFE	Objective Function Evaluation
SA	Simulated Annealing
SD	Standard Deviation

SGA Search Group Algorithm

SVM Support Vector Machine



# List of symbols

## Capital Latin Symbols

$A$	Axle load
$A_s$	Reinforcement section area
$A_{ss}$	Stiffener area
$A_t$	Area of the stiffener
$A_{t_{min}}$	Minimum area of the stiffener
$B_{bridge}$	Width of the bridge
$B$	Strain-displacement matrix
$B_b$	Bending strain-displacement matrix
$B_s$	Transverse shear strain-displacement matrix
$Cost$	Cost function
$C$	Matrix of constitutive relations
$C_b$	Bending constitutive matrix
$C_s$	Transverse shear constitutive matrix
$D_c$	Depth of the web in compression in the elastic range
$E$	Elastic modulus
$F$	Random value
$F_{cr}$	Critical buckling stress for plates
$F_{sa}$	Stiffener allowable stress

$F_v$	Allowable shear stress on the beam web
$F_{ve}$	Shear stress on the transversal stiffener
$G$	Shear modulus
$I_s$	Inertia of the longitudinal stiffener
$I_{smin}$	Minimum inertia of the longitudinal stiffener
$I_t$	Inertia of the transversal stiffener
$I_{tmin}$	Minimum inertia of the transversal stiffener
$I_y$	Moments of inertia about the minor principal axis of the cross-section
$I_{yc}$	Moment of inertia of the compression flange of a steel section about the vertical axis in the plane of the web
$J$	Objective function
$J_t$	Torsional inertia
$K_b$	Plate bending stiffness matrix
$K_g$	Stiffness global matrix
$K_m$	Membrane stiffness matrix
$K_p$	Plate stiffness matrix
$K_s$	Plate transverse shear stiffness matrix
$K_{shell}$	Shell stiffness matrix
$L$	Matrix of differential operators
$L_b$	Bridge free span
$M$	Bending moment

$M_n$	Nominal flexural resistance based on the tension flange
$M_u$	Moment due to factored loads
$\mathbf{N}$	Matrix of shape functions
$\mathbf{N}\mathbf{a}(\xi, \eta)$	Parametric coordinates matrix
$NA$	Neutral axis
$N_i$	Shape functions
$OF_{FEM}^{max}$	Maximum objective function evaluations for the FEM model
$OF_{SM}^{max}$	Maximum objective function evaluations for each iteration of the simplified model
$P$	Tire load
$Pop$	Population created in the Initialization process
$R_{ij}$	Former $j^{th}$ column of the search group matrix
$S$	Project admissible region
$\mathbf{T}_b$	Bending subdivision of the transformation matrix
$\mathbf{T}_B$	Transformation matrix
$T.C._n$	Total cost of the $n^{th}$ empire
$\mathbf{T}_M$	Mindlin transformation matrix
$\mathbf{T}_s$	Shear subdivision of the transformation matrix
$V$	Design shear force on the support
$V_{d1}$	Shear due to the factored loads considering the presence of a transversal stiffener
$V_n$	Nominal shear resistance

$V_{n,sup}$	Support stiffener nominal shear resistance
$V_u$	Shear due to the factored loads
$\mathbf{X}^{*k}$	Final population of the $k^{th}$ iteration of the simplified model
$\mathbf{X}^k$	Population of the $k^{th}$ iteration of the simplified model
$\mathbf{X}^{*opt}$	Best individual of each iteration of the simplified model

### Lower Case Latin Symbols

$\mathbf{a}$	Polynomial parameters vector
$a_i$	Polynomial parameters
$b_2$	Width between beams
$b_s$	Beam top flange width
$b_{sa}$	Support stiffener width
$b_{sl}$	Longitudinal stiffener width
$b_{st}$	Transversal stiffener width
$b_u$	Width of the bottom flange of the beam
$c$	Factor
$\mathbf{d}$	Vector of nodal DOF
$d_0$	Distance between the support and the first transversal stiffener
$d_1$	Distance between each transversal stiffener
$d_{comp}$	Distance from compression face to centroid of tension reinforcement

$diaf$	Profile of diaphragms
$d_{stud}$	Stud diameter
$dv_q$	Possible discrete values for the variables
$e$	Eccentricity between slab and beam axis
$\mathbf{f}$	Nodal forces vector
$f_{bi}$	Bottom flange maximum stress
$f_{bs}$	Top flange maximum stress
$f'_c$	Concrete 28-day compressive strength
$f_c$	Slab maximum stress
$f_{c omp}$	Compression-flange stress at the section under consideration
$\mathbf{f}_g$	Force global vector
$\mathbf{f}_p$	Surface tractions vector
$\mathbf{f}_q$	Body forces vector
$f_v$	Beam web maximum stress
$f_y$	Steel yield strength
$f_{ya}$	Allowable yield strength of the steel
$g_j$	Inequality restrictions
$h$	Deck thickness
$h_j$	Equality restrictions
$h_{stud}$	Stud height
$h_v$	Beam web height

$it_{SM}^{max}$	Maximum iterations of the simplified model
$j$	Factor
$k$	Factor defined by the slab height
$\mathbf{k}_b$	Mindlin curvature sub-vector
$\mathbf{k}_M$	Mindlin curvature and transverse shear strain vector
$\mathbf{k}_s$	Mindlin transverse shear strain sub-vector
$k_t$	Torsional spring constant
$k_v$	Vertical spring constant
$m(x)$	Uniform distributed torsion moment
$n_{diaf}$	Number of diaphragms used
$n_{pop,FEM}$	Size of the population used in the FEM model
$n_{pop,SM}$	Size of the population used in the simplified model
$oldP$	Historical population
$\mathbf{p}$	Surface tractions vector
$p$	Bridge uniform load
$p(x)$	Uniform loading
$p_i^*$	Standard bound
$p_i$	Given structural response
$\mathbf{q}$	Body forces vector
$r_{diaf}$	Radius of gyration of the diaphragm section
$r_{ij}$	Cartesian distance between the two fireflies
$t$	Plate height

$t_s$	Beam top flange thickness
$t_{sa}$	Support stiffener thickness
$t_{sl}$	Longitudinal stiffener thickness
$t_{st}$	Transversal stiffener thickness
$t_u$	Thickness of the bottom flange of the beam
$t_w$	Beam web thickness
$\mathbf{u}$	Displacements vector
$u(x)$	Displacements function
$u(\xi, \eta)$	Parametric displacement $u$
$\mathbf{u}(\xi, \eta)$	Parametric displacements vector
$u_i$	Translation in direction $x$
$u_{xb}$	Beam nodal displacement in $x$
$u_{xp}$	Plate nodal displacement in $x$
$u_{zb}$	Beam nodal displacement in $z$
$u_{zp}$	Plate nodal displacement in $z$
$v(x)$	Displacements function
$v(\xi, \eta)$	Parametric displacement $v$
$v_i$	Translation in direction $y$
$w$	Vertical displacement
$w(x)$	Displacements function
$w_i$	Translation in direction $z$
$w_{par}$	Positive weight parameter

$x$	Design variables
$\mathbf{x}^*$	Optimum design
$x_d$	Discrete variables
$x_j^{new}$	Perturbed individual
$x_k$	Continuous variables
$\mathbf{x}_i^k$	Members of the simplified model population
$\mathbf{x}_{FEM}^{*opt}$	Best individual found in the FEM model stage
$\mathbf{x}_{SM}^{*opt}$	Optimum design of the first stage

## Greek Symbols

$\alpha_{FA}$	Randomization parameter
$\alpha_i$	Polynomial parameters
$\alpha_{SGA}$	Parameter that controls the size of the perturbation
$\beta_0$	Attractiveness at $r = 0$
$\gamma$	Light absorption coefficient
$\Delta$	Deflection
$\delta \mathbf{d}$	Virtual nodal DOF vector
$\delta \mathbf{u}$	Virtual displacement vector
$\delta \boldsymbol{\varepsilon}$	Virtual strain vector
$\delta \boldsymbol{\varepsilon}_b(\xi, \eta, z)$	Bending virtual strain vector
$\delta \boldsymbol{\varepsilon}_s(\xi, \eta)$	Transversal shear virtual strain vector
$\boldsymbol{\varepsilon}$	Strain vector



$\boldsymbol{\varepsilon}_b$	Vector of strains
$\varepsilon_r$	Random variable
$\boldsymbol{\varepsilon}_r$	Random vector
$\boldsymbol{\varepsilon}_s$	Vector of shear deformations
$\varepsilon_x$	Strain in the x direction
$\varepsilon_y$	Strain in the y direction
$\varepsilon_z$	Strain in the z direction
$\eta$	Parametric coordinate
$\theta$	Torsion angle
$\theta_x(x)$	Displacements function
$\theta_{xi}$	Rotation around the x axis
$\theta_{yb}$	Beam nodal rotation around y
$\theta_{yi}$	Rotation around the y axis
$\theta_{yp}$	Plate nodal rotation around y
$\theta_{zi}$	Rotation around the z axis
$\lambda_{xy}$	Shear deformation in the xy plane
$\lambda_{xz}$	Shear deformation in the xz plane
$\lambda_{yz}$	Shear deformation in the yz plane
$\nu$	Poisson coefficient
$\xi$	Parametric coordinate
$\xi_1$	Positive number which is considered to be less than 1
$\rho$	Reinforcement steel rate

$\sigma$	Stress vector
$\sigma_c$	Slab normal stress
$\tau_R$	Concrete shear stress resistance
$\tau_s$	Slab shear stress
$\varphi$	Impact factor

# Summary

<b>List of Figures</b> . . . . .	<b>17</b>
<b>List of Tables</b> . . . . .	<b>19</b>
<b>1 Introduction</b> . . . . .	<b>35</b>
1.1 Motivation . . . . .	35
1.2 Literature Review . . . . .	38
1.3 Scope and Objective of the Study . . . . .	41
1.4 Organization of the Text . . . . .	42
<b>2 Steel-Concrete Composite I-Girder Bridges</b> . . . . .	<b>45</b>
2.1 Bridge Structural Design . . . . .	45
2.1.1 Loads . . . . .	47
2.1.2 Design Constraints - Allowable Stresses . . . . .	49
2.1.3 Design Constraints - Limit and Resistance Factor Design . . . . .	55
2.2 Structural Analysis . . . . .	57
2.2.1 Simplified Models . . . . .	58
2.2.2 Finite Element Model (FEM) . . . . .	61
<b>3 Fundamentals of Optimization</b> . . . . .	<b>73</b>
3.1 General Concepts . . . . .	73
3.2 Algorithms . . . . .	76
3.2.1 Backtracking Search Algorithm (BSA) . . . . .	76
3.2.2 Firefly Algorithm (FA) . . . . .	78
3.2.3 Genetic Algorithm (GA) . . . . .	78
3.2.4 Imperialist Competitive Algorithm (ICA) . . . . .	80
3.2.5 Search Group Algorithm (SGA) . . . . .	81
3.3 Statistic Tests . . . . .	83
<b>4 Steel-Concrete Composite I-Girder Bridge Optimization</b> . . . . .	<b>89</b>
4.1 Optimization Problem . . . . .	89
4.2 Two-Stage Based Optimization Approach . . . . .	94
<b>5 Numerical Example</b> . . . . .	<b>99</b>

5.1	Structure Studied . . . . .	99
5.2	Mechanical Model Validation . . . . .	100
5.3	Assessment of the Heuristic Algorithms . . . . .	105
5.4	Two-stage Bridge Optimization . . . . .	108
5.4.1	Allowable Stresses . . . . .	109
5.4.2	Limit and Resistance Factor Design . . . . .	111
<b>6</b>	<b>Concluding Remarks and Future Developments . . . . .</b>	<b>117</b>
6.1	Concluding Remarks . . . . .	117
6.2	Future Studies . . . . .	119
	<b>References . . . . .</b>	<b>121</b>
	<b>Annex . . . . .</b>	<b>129</b>
	<b>Annex A Rüsçh's tables . . . . .</b>	<b>131</b>

# Chapter 1

## Introduction

### 1.1 Motivation

Historically, bridges arose by the necessity of people to cross rivers and valleys. The ancient Romans are recognized as the first builders able to construct bridges with reasonable spans and withstanding conditions that would damage previous designs. Their oldest bridge is the so-called Fabricio Bridge (Figure 1), located in Rome. It still is in existence until today, presenting a 24.5m span.

The iron was first employed in 1779, in a 31m span arch structure in England. Since then, the materials and techniques used in the construction evolved significantly. The modern suspension bridges and the first concrete bridges started to be designed in the 19<sup>th</sup> century. Among the former, the Brooklyn Bridge was constructed in 1870, presenting 480m of free span. The 20<sup>th</sup> century consolidated the use of cable-stayed structures, which becomes economical for big spans.

Within this context, the steel-concrete composite bridges started to be designed in the 30's of the last century. They are formed with a concrete deck and steel beams, which can be I-sections or box girders. According to Chen, Duan & Altman (2000), the latter are usually employed in the construction of urban highway, horizontally curved and long-span bridges. They have higher flexural capacity, torsional rigidity



Figure 1 – Fabricio bridge, Rome - Italy

and the closed shape reduces the exposed surface, making them less susceptible to corrosion. The Pedro Ivo Campos Bridge, that links the continental part of Florianópolis to the Santa Catarina Island (Figure 2), is a typical example of this bridge solution.



Figure 2 – Pedro Ivo Campos bridge, Florianópolis - Brazil

The steel-concrete composite I-girder bridge systems are often the most economical solution to simply supported straight axis structures.

In practical applications, its span usually varies from 20 to 50m. The Perimetral Viaduct (Figure 3), in Rio de Janeiro, is an example of an I-section composite structure.



Figure 3 – Perimetral viaduct, Rio de Janeiro - Brazil

The importance of composite bridges can be verified by its great number of studies, for instance, Madrazo-Aguirre, Ruiz-Teran & Wadee (2015), Liu et al. (2014) and Zhou et al. (2016) discussed the dynamic repercussions on these structures. The design and the structural analysis are topics for Liu et al. (2009) and Ellobody (2014). Also, Oehlers (1990) focused on stud deterioration and Gocál & Ďuršová (2012) made an optimization parametric study, just to name a few. Considering the Brazilian researchers, steel-concrete composite bridges has been studied by Pinho & Bellei (2007), Fernandes (2008) and Klinsky (1999), who discussed bridge design as well as its structural behavior. Leitão et al. (2011) assessed the bridge fatigue. It can be cited Vitória (2015) as a contributor to discuss the conservation, damage and strengthening of

these structures. Also, Fabiane (2015) with main focus on optimization directrices.

Despite the reasonable amount of research, those investigations are not dealing with full optimization studies. In addition, even considering the relative simple configuration of composite bridges, the final solution strongly depends on the engineer experience due to the great number of design variables. Therefore, it is intended to achieve better economical solutions with the help of optimization procedures.

## 1.2 Literature Review

The structural optimization is a very relevant field and has been a growing focus on research. Initial emphasis had been given to truss structures and some important advances were carried out - Tang, Tong & Gu (2005), Kelesoglu (2007), Rahami, Kaveh & Gholipour (2008), Torii, Lopez & Biondini (2012), Miguel, Lopez & Miguel (2013), Wang & Ohmori (2013) and Torii, Lopez & Miguel (2014), just to name a few. However, it is essential to note that the main focus of these studies was the implementation and development of different optimization procedures applied only to academic examples of truss structures.

In the context of industrial application of complex 3D structures with a large number of members and subjected to several constraints imposed by standard design codes, the number of existing studies in the literature is reduced - Shea & Smith (2006), Guo & Li (2011), Kripka, Medeiros & Lemonge (2015), Munck et al. (2015), Huang et al. (2015), Kaveh & Behnam (2013), Sharafi, Teh & Hadi (2014), Kociecki & Adeli (2013), Kravanja et al. (2013), Poitras, Lefrançois & Cormier (2011), Kaveh & Abadi (2010), Lopez, Luersen & Cursi (2009), Haftka (1989), Kodiyalam & Vanderplaats (1989), Vanderplaats (1999), Arora (2004), Taniwaki & Ohkubo (2004), Bhatti (1999), Balling, Briggs & Gillman (2006), Lee & Geem (2005), Bartholomew & Morris (1976), Furukawa et al. (1989), Qin (1992) and Yang (1997). The main issues are related to constructive feasibility of the optimum algorithm solution and the



compatibility of the structural behavior between the model and the actual structure, as showed in Souza et al. (2015).

Some works addressing bridge optimization, which take into account the principal aspects to some degree, can also be found in literature. Lute, Upadhyay & Singh (2009) proposed a new approach combining a Genetic Algorithm (GA) and support vector machine (SVM) to carry out the optimization design of cable-stayed bridge structures. The proposed framework consists of a two-phase operation. In the first phase, the training data are generated using FEM analysis routine which are used for the learning process of a SVM regression machine. In the second phase, GA and SVM are combined to get a hybrid tool for optimization of cable-stayed bridges. As the main advantage, the computation time of optimization is reduced.

Cai & Aref (2015) studied the use of carbon fiber reinforced polymeric (CFRP) materials in the cable system of a cable-stayed bridge. This work used a GA-based optimization process to improve the aerodynamics of the cable system. The analysis of the structure checked the static, dynamic and flutter performances of the bridge.

Martins, Simões & Negrão (2015) applied a gradient based approach (*fmincon* function on Matlab) to optimize the cable forces on stay-cabled bridges. This work included the analysis of concrete time-dependent effects, the construction sequence and the geometrical nonlinearities. The structure of the tower and deck of the bridge were modeled as a 2-node Euler-Bernoulli beam elements, and the stay as a 2-node bar element.

Baldomir et al. (2010) optimized the cross-sectional areas of the stay cables of a cable-stayed bridge in the design phase. The structure was modeled as a 3-node bar elements using the software Abaqus. The optimization was also carried out by a gradient based approach. However, as pointed out by Hassan (2013), due to the local characteristic of the optimization procedure employed, the final solution found by Baldomir et al. (2010) may not be the global minimum. In Hassan (2013), the author developed a design optimization technique in order to achieve the

minimum cross-sectional areas of stay cables. The technique integrated finite element method, B-spline curves, and genetic algorithm. The capability and efficiency of the proposed optimization technique was tested and assessed by applying it to a practical sized cable-stayed bridge.

Kusano et al. (2014) investigated the reliability based design optimization of long-span bridges considering flutter. Uncertainties in extreme wind velocity as well as flutter derivatives obtained in wind tunnel were taken into account.

Cheng (2010) studied the optimal design of steel truss arch bridges. The proposed algorithm integrated the concepts of the GA and the finite element method. The objective function was the weight of the structure, strength (stress) and serviceability (deflection) constraints were considered. The bridge was modeled by a 2D-truss element and the finite element model contained 465 elements and 228 nodes. Cheng, Qian & Sun (2013) carried out a gradient based scheme on a linear finite element model for the structure analysis.

Martí et al. (2013) developed an optimization algorithm to minimize the cost of prestressed concrete precast road bridges based on the Simulated Annealing (SA). The entire set of the bridge variables was optimized and a 20-bar structural model was used for the structure analysis.

Kaveh, Maniat & Naeini (2016) optimized the superstructure of post-tensioned concrete bridges using a modification of the metaheuristic algorithm Colliding Bodies Optimization (CBO). This study used 135 AASHTO and construction constraints to optimize 17 geometric design variables. The results were compared to two others optimization algorithm.

The study of Martínez et al. (2011) consisted on finding the optimum design for piers of tall bridges using the Ant Colony Optimization (ACO). In this article, the actions used to design the pier were considered fixed parameters.

For composite bridges, there is the work of Gocál & Ďuršová

(2012), who made a parametric study to optimize the transversal disposition of the beams on a steel-concrete composite I-girder bridge. It modeled 32 possible structures with the SCIA Engineer software and analyzed the consumption of steel and concrete of each design. It was not found any article in the literature dealing with the full optimization of steel-concrete composite I-girder bridges.

Also, the optimization of composite I-girder bridges developed in this dissertation was published on Pedro et al. (2017).

### 1.3 Scope and Objective of the Study

The main objective of this dissertation is to study the design optimization of steel-concrete composite I-girder bridges. Thus, this dissertation proposes an efficient two-stage optimization based approach to design this kind of structures. In the first stage, a simplified structural model, usually adopted by bridge designers, is employed pursuing to locate an optimum region and to provide a starting point to the next search. Then, a complete finite element model (FEM) using frame and shell elements is used to refine and improve the optimization.

Due to the complexity of the optimization problem and the high computational cost of a full FEM model for the bridge, the main advantage of the proposed two-stage approach is its ability of combining the benefits furnished by each stage. The first step requires a very low computational time. Then, the optimization algorithm can be repeated a great number of times, without much increase in the processing time. Thus, only the best design is selected and used as a member of the population of the second stage. This stage is more precise, but also more computationally demanding. Through this procedure, the optimum design can follow an accurate structural model while using a reasonable computational processing.

Because of the problem nature and due to the presence of discrete variables, the optimization is conducted through five well-known meta-heuristic algorithms: Backtracking Search Algorithm (BSA), Firefly

Algorithm (FA), Genetic Algorithm (GA), Imperialist Competitive Algorithm (ICA) and Search Group Algorithm (SGA). The latter was recently developed by Gonçalves, Lopez & Miguel (2015) which is showing very promising results in different engineering applications. To assess the algorithm that better suits the problem, a performance analysis through statistics tests is carried out.

Specific objectives can be also listed:

- to develop an efficient optimization tool to be used as an accessory to steel-concrete composite I-girder bridge designers;
- to compare, statistically, the efficiency of five well known meta-heuristic algorithms for the steel-concrete composite I-girder bridge optimization;
- to compare the simple model usually adopted by designers with a more refined methodology;
- to assess the influence of a most modern design philosophy (Load and Resistance Factor Design vs Allowable Stress Design ) on the optimum results.

## 1.4 Organization of the Text

The dissertation is divided in 6 chapters. This, which is the first one, aims to introduce and to delimit the research scope.

The second chapter presents a general description of steel-concrete composite I-girder bridges and describes the general methodology used to its structural design.

The third chapter presents an overview on engineering optimization. The main definitions are presented, as well as the heuristic algorithms used in this dissertation. Finally the statistic tests used to compare the efficiency between algorithms are explained.

The fourth chapter details the steel-concrete optimization problem. It shows its variables and formulations as well as the optimization approach to find the optimum solution.

The fifth chapter presents the numerical examples used to test the optimization approach developed. For this purpose, a composite bridge previously studied in Pinho & Bellei (2007) and Leitão et al. (2011) is assessed. Firstly, a validation procedure is carried out aiming to guarantee the appropriate behavior of the FEM bridge model. Then, the composite bridge is optimized by five heuristic algorithms. This optimization is pursued using the Level Rule and its objective is to assess the best algorithm for this specific problem. Afterwards, the composite bridge is designed using the proposed two-stage based optimization approach. In this part, two classical simplified models (Level Rule and Fauchart) are used to compare its performance. Finally, because the original design was studied prior the newest AASHTO standard it employed the Allowable Stress Design (ASD) approach, the bridge is also optimized through the Limit and Resistance Factor Design (LRFD) method, to demonstrate the influence of a most modern design philosophy on the obtained results.

Finally, the sixth chapter presents the concluding remarks and the suggestions for future developments of this work.



## Chapter 2

# Steel-Concrete Composite I-Girder Bridges

This chapter presents a general description of steel-concrete composite I-girder bridges as well as describes the general methodology used to its structural design. First, the loads acting on the structure are detailed. Then, the structural constraints imposed by AASHTO (2002) are described. Finally, the two structural models used to represent the bridge are discussed. For further details on this subject, the reader is referred to Pinho & Bellei (2007), Chen, Duan & Altman (2000) and the references therein.

### 2.1 Bridge Structural Design

The steel-concrete composite I-girder bridges are usually constructed adopting rolled or built-up (plate girder) I-sections. Due to its limited dimensions, rolled I-sections are most applicable to shorter span (up to 30m) bridges. Plate girders are composed by top and bottom flanges welded to a web plate with dimensions determined according to the specific design. Therefore, higher transversal sections can be constructed, allowing their use to longer span bridges (above 30m).

This plate girder feature provides to the bridge designer flexibility

to determine the flanges and web plates dimensions efficiently. They must present adequate strength without resulting in any additional manufacturing difficulties. Depending on the web slenderness, it must be employed web transverse and longitudinal stiffeners. The former provides a tension-field action increasing the post-buckling shear strength and the latter allows developing inelastic flexural buckling strength. Then, the engineer must define the cross sectional dimensions that meets safety and constructional requirements while looking to its minimum weight.

According to Chen, Duan & Altman (2000), simple rules can be used as a first attempt to determine web and flange dimensions:

- **Webs:** The web mainly provides shear strength for the girder. The web height is commonly taken as  $1/18$  to  $1/20$  of the girder span length for highway bridges and slightly less for railway bridges. Since the web contributes little to the bending resistance, its thickness should be as small as local buckling tolerance allows. Transverse stiffeners increase shear resistance by providing tension field action and are usually placed near the supports and large concentrated loads. Longitudinal stiffeners increase flexure resistance of the web by controlling lateral web deflection and preventing the web bending buckling. They are, therefore, attached to the compression side. It is usually recommended that sufficient web thickness be used to eliminate the need for longitudinal stiffeners as they can create difficulty in fabrication. Bearing stiffeners are also required at the bearing supports and concentrated load locations and are designed as compression members.
- **Flanges:** The flanges provide bending strength. The width and thickness are usually determined by choosing the area of the flanges within the limits of the width-to-thickness ratio and the requirement as specified in the design specifications to prevent local buckling. Lateral bracing of the compression flanges is usually needed to prevent lateral torsional buckling during various load stages.



In summary, a steel-concrete composite I-plate girder bridge is basically composed by the concrete slab, the steel I-section beams and the accessories (stiffeners, diaphragms and shear connectors). The shear connectors usually employed in bridges are the studs, and they have the function to connect the slab and girder, giving the structure a complete interaction. To better understand the nomenclature, Figures 4 and 5 show a composite bridge and its parts, respectively.

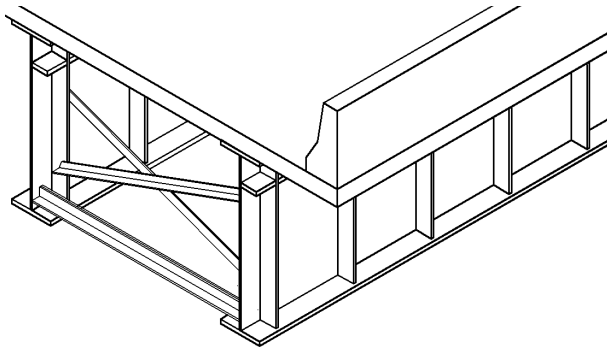


Figure 4 – Steel-concrete composite I-girder bridge

### 2.1.1 Loads

The bridges must be designed to withstand permanent, accidental and moving loads. The permanent load is calculated from the self-weight of the pavement, the structure and other bridge accessories, for instance the traffic barriers. To obtain the stress on the beams, this permanent load is also divided in before and after the concrete curing. This division is important, because the beams are composite structures. Thus, the self-weight of the structure (beams and slab) has to be resisted by the steel beam alone (non-composite structure). However, the pavement and traffic barriers load will be resisted by the steel-concrete beam system (composite structure).

The accidental load is taken into account as the hypothesis of a car collision with the traffic barrier. For that consideration, it is applied

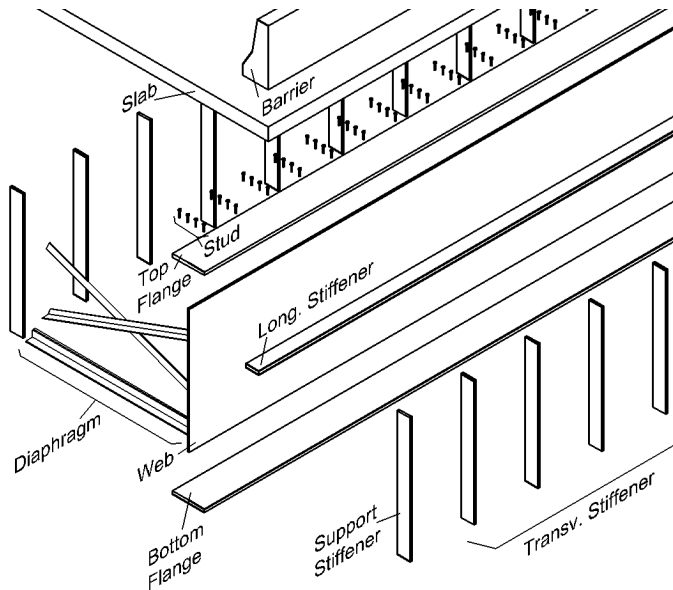


Figure 5 – Parts of a steel-concrete composite I-girder bridge

a horizontal force of 60kN on the top edge of the barrier. This load can have its stresses distributed throughout the barrier and the deck in 45 degrees and has to be applied only if it is greater than the moving load.

For the moving load, it is employed the vehicle model indicated on the NBR 7188 (ABNT, 1984) "TB-45"(Figure 6). This design truck corresponds to three 150kN axles spaced 1.5m apart, denominated as load *A*. The tire load, *P*, is 75kN spaced 2m apart in the transversal direction. The vehicle tire loadings are accompanied by uniform loading, *p*, of 5kN/m<sup>2</sup>. The location of the moving load is switched on the bridge to find the worst stress scenario to the beams and the slab. This allows determining the stress envelope to design the geometry of all girders equally, which will resist this load as a composite structure. This adopted procedure, which is usually employed by bridge engineers, is exactly the same applied in the original design of the studied bridge. In addition, the impact factor, calculated by Equation 2.1 - according to NBR 7187

(ABNT, 2003) -, is also taken into account.

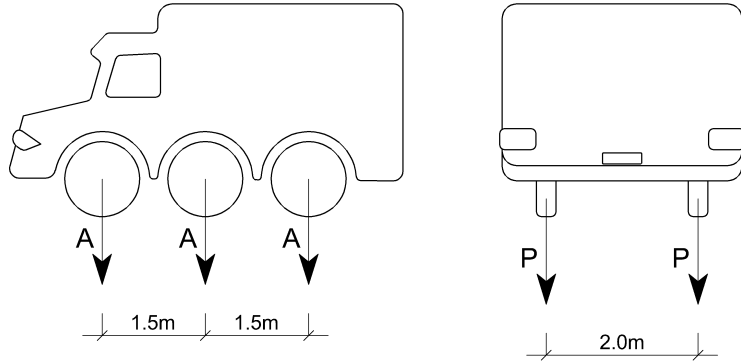


Figure 6 – Vehicle TB-45

$$\varphi = 1.4 - 0.007 \times L_b[m] \quad (2.1)$$

where  $\varphi$  is the impact factor and  $L_b$  is the span of the bridge.

### 2.1.2 Design Constraints - Allowable Stresses

The structural constraints used in this study follow the AASHTO standard recommendations (AASHTO, 2002). All the steel required failure and serviceability checks are carried out using the allowable stresses methodology as presented below. Once again, all these checks are the same adopted in the original bridge design.

#### a) Slab

##### Reinforcement Steel

The slab reinforcement is calculated in both directions considering the positive and negative bending moments. Its constraint is demonstrated in Equation 2.2.

$$A_s \geq \frac{M}{f_{ya} \times (d_{comp} - 0.4 \times NA)} \quad (2.2)$$

where  $A_s$  is the reinforcement section area;  $M$  is the greatest bending moment on the slab;  $f_{ya}$  is the allowable yield strength of the steel;  $d_{comp}$  is the distance from compression face to centroid of tension reinforcement;  $NA$  is the section neutral axis.

### Shear

The shear stress in the slab is calculated in the moving load most critical position and is verified by Equation 2.3.

$$\tau_s \leq \tau_R \times k(1.2 + 40\rho) + 0.15\sigma_c \quad (2.3)$$

where  $\tau_s$  is the slab shear stress;  $\tau_R$  is the concrete shear stress resistance;  $k$  is a factor defined by the slab height;  $\rho$  is the reinforcement steel rate;  $\sigma_c$  is the slab normal stress.

### Maximum Deflection

The maximum vertical deflection is calculated (considering a linear elastic model) in mid-span for the central slab and in the edge for the lateral cantilever. Their corresponding limit values are defined in Equation 2.4 and 2.5, respectively.

$$\Delta \leq \frac{L_b}{800} \quad (2.4)$$

$$\Delta \leq \frac{L_b}{300} \quad (2.5)$$

where  $\Delta$  is deflection in mid-span or in the edge of the lateral cantilever;  $L_b$  is the span length.

## **b) Girders**

### Allowable Stress

Equations 2.6, 2.7, 2.8 and 2.9 are applied to define the allowable stresses in the structure.

$$f_{bs} \leq 0.55 \times f_y \quad (2.6)$$

$$f_{bi} \leq 0.55 \times f_y \quad (2.7)$$

$$f_v \leq 0.33 \times f_y \quad (2.8)$$

$$f_c \leq 0.40 \times f'_c \quad (2.9)$$

where  $f_{bs}$ ,  $f_{bi}$  and  $f_c$  are the maximum normal stresses on the top and bottom flange and slab, respectively;  $f_v$  is the maximum shear stress on the beam web;  $f_y$  is the yield strength of the steel;  $f'_c$  is the 28-day compressive concrete strength.

As explained in Section 2.1.1, the self-weight of the structure (beams and deck) has to be resisted by the steel beam alone (non-composite structure). However, the pavement and traffic barriers load will be resisted by the steel-concrete beam system (composite structure).

#### Maximum Deflection

The maximum deflection is calculated in mid-span with corresponding value defined by Equation 2.10.

$$\Delta \leq \frac{L_b}{800} \quad (2.10)$$

Again, the girder deflections must be verified at the construction stage (non-composite structure) as well as in the final composite configuration.

### **c) Accessories**

#### Shear Connector

The number of studs, used as shear connectors, is determined based on fatigue considerations and the shear stress on the bridge section. In addition, it has two size constraints to be followed (Equations 2.11 and 2.12)

$$h_{stud} \geq 4 \times d_{stud} \quad (2.11)$$

$$d_{stud} \leq 2.5 \times t_s \quad (2.12)$$

where  $h_{stud}$  and  $d_{stud}$  are the height and diameter of the stud;  $t_s$  is the beam top flange thickness.

### Support Stiffener

The support stiffener is defined by the following constraints.

$$b_{sa} \leq \frac{b_s - t_w}{2} \quad (2.13)$$

$$t_{sa} \geq \frac{b_{sa}}{12} \sqrt{\frac{f_y}{22.8 \left[ \frac{kN}{cm^2} \right]}} \quad (2.14)$$

$$F_{sa} \geq \frac{V}{A_{ss}} \quad (2.15)$$

where  $b_{sa}$  and  $t_{sa}$  are the width and thickness of the support stiffener;  $b_s$  is the beam top flange width;  $t_w$  is the beam web thickness;  $F_{sa}$  is the stiffener allowable stress;  $V$  is the design shear force on the support;  $A_{ss}$  is the area of the stiffener.

### Transversal Stiffener

The transversal stiffeners shall be employed when the following Equations 2.16, 2.17 and 2.18 are satisfied.

$$t_w \leq \frac{h_v}{150} \quad (2.16)$$

$$f_v \geq F_{ve} \quad (2.17)$$

$$F_{ve} \leq F_v \quad (2.18)$$

where  $h_v$  is the beam web height;  $F_{ve}$  is the shear stress on the transversal stiffener;  $F_v$  is the allowable shear stress on the beam web.

When the use of transversal stiffeners is necessary, its size is defined following the constraints in Equations 2.19, 2.20, 2.21, 2.22 and 2.23.

$$b_{st} \geq 5 + \frac{h_v}{30[cm]} \quad (2.19)$$

$$b_{st} \geq \frac{b_s}{4} \quad (2.20)$$

$$t_{st} \geq \frac{b_{st}}{16} \quad (2.21)$$

$$At \geq At_{min} = [0.15 \frac{h_v}{t_w} (1 - c) \frac{f_v}{F_{cr}} - 18] \frac{f_y}{F_{cr}} t_w^2 \quad (2.22)$$

$$It \geq It_{min} = d_1 \times t_w^3 \times j \quad (2.23)$$

where  $b_{st}$  and  $t_{st}$  are the width and thickness of the transversal stiffener;  $At$  and  $At_{min}$  are the area and the minimum area of the stiffener;  $c$  is a factor equal 1 for a pair of stiffeners;  $F_{cr}$  is the critical buckling stress for plates;  $It$  and  $It_{min}$  are the inertia and the minimum inertia of the stiffener;  $d_1$  is the distance between each transversal stiffener;  $j$  is a factor defined by  $j = 2.5(\frac{h_v}{d_1})^2 - 2 \geq 0.5$ .

### Longitudinal Stiffener

Similarly as for the transversal stiffener, the algorithm first detects the necessity of the longitudinal stiffener using Equations 2.24 and 2.25.

$$t_w \leq \frac{h_v}{170} \quad (2.24)$$

$$t_w \leq h_v \frac{\sqrt{f_{bs}}}{600} \quad (2.25)$$

If the use is necessary, then the stiffener is defined following the constraints in Equations 2.26, 2.27, 2.28 and 2.29.

$$b_{sl} \geq 5 + \frac{h_v}{30[cm]} \quad (2.26)$$

$$b_{sl} \geq \frac{b_s}{4} \quad (2.27)$$

$$t_{sl} \geq \frac{b_{sl}}{16} \quad (2.28)$$

$$I_s \geq I_{s_{min}} = h_v \times t_w^3 [2.4 \frac{d_1^2}{h_v^2} - 0.13] \quad (2.29)$$

where  $b_{sl}$  and  $t_{sl}$  are the width and thickness of the longitudinal stiffener;  $I_s$  and  $I_{s_{min}}$  are the inertia and the minimum inertia of the stiffener.

When using this stiffener it is important to check the beam web using the constrains defined by Equations 2.30 and 2.31.

$$t_w \leq \frac{h_v}{340} \quad (2.30)$$

$$t_w \leq h_v \frac{\sqrt{f_{bs}}}{1200} \quad (2.31)$$

### Diaphragm

The diaphragms are checked by its slenderness and maximum spacing (Equations 2.32, 2.33 and 2.34).

$$n_{diaf} \geq \frac{L_b}{7.6} + 1 \quad (2.32)$$

$$r_{diaf} \geq \frac{1}{2} \frac{b_2}{120} \quad (2.33)$$

$$r_{diaf} \geq \frac{\sqrt{b_2^2 + (t_s + h_v + t_i)^2}}{200} \quad (2.34)$$

where  $n_{diaf}$  is the number of diaphragms used;  $r_{diaf}$  is the perpendicular radius of gyration of the diaphragm section;  $b_2$  is the width between beams.



### 2.1.3 Design Constraints - Limit and Resistance Factor Design

Aiming to consider the influence of the design methodology in the optimum results, it will be also employed the AASHTO (2012) LRFD based approach. The checks for failure and serviceability of this methodology are listed below.

#### a) Slab

##### Reinforcement Steel

The slab reinforcement is calculated in both directions considering the positive and negative bending moments. Its constraint is demonstrated in Equation 2.35.

$$A_s \geq \frac{M_u}{f_y \times (d_{comp} - 0.4 \times NA)} \quad (2.35)$$

where  $M_u$  is the moment due to factored loads.

#### b) Girder

##### Limit and Resistance Factor Design

Equations 2.36 to 2.40 are applied to define the structure.

$$M_u \leq M_n \quad (2.36)$$

$$I_{yc} \leq 0.9 \times I_y \quad (2.37)$$

$$I_{yc} \geq 0.1 \times I_y \quad (2.38)$$

$$\frac{b_s}{2t_s} \leq 1.38 \sqrt{\frac{E_s}{f_{comp} \sqrt{\frac{2D_c}{tw}}}} \quad (2.39)$$

$$V_{d1} \leq V_n \quad (2.40)$$

where  $M_n$  is the nominal flexural resistance based on the tension flange;  $I_{yc}$  is the moment of inertia of the compression flange of a steel section

about the vertical axis in the plane of the web;  $I_y$  is the moments of inertia about the minor principal axis of the cross-section;  $f_{c,omp}$  is the compression-flange stress at the section under consideration;  $D_c$  is the depth of the web in compression in the elastic range;  $V_{d1}$  is the shear due to the factored loads considering the presence of a transversal stiffener;  $V_n$  is the nominal shear resistance.

### c) Accessories

#### Support Stiffener

The support stiffener shall be employed when the following Equation is satisfied:

$$V_u \geq V_n \quad (2.41)$$

After verifying its need, it is defined by the following constraints.

$$V_u \leq V_{n,sup} \quad (2.42)$$

$$b_{sa} \geq 0.25 \times b_s \quad (2.43)$$

$$b_{sa} \leq 0.48 \times t_{sa} \sqrt{\frac{E_s}{f_y}} \quad (2.44)$$

$$b_{sa} \leq 16 \times t_{sa} \quad (2.45)$$

$$b_{sa} \geq 2 \times 2.54 + \frac{h_v}{30[cm]} \quad (2.46)$$

where  $V_u$  is the shear due to the factored loads;  $V_{n,sup}$  is the support stiffener nominal shear resistance.

#### Transversal Stiffener

The transversal stiffeners, as the support stiffener, also shall be employed when the Equation 2.41 is satisfied. Its design follows the

same rules as the support stiffener.

#### Longitudinal Stiffener

Similarly as for the other stiffeners, the algorithm first detects the necessity of the longitudinal stiffener using Equation 2.47.

$$2 \frac{D_c}{tw} \geq 6.77 \sqrt{\frac{E_s}{f_{c omp}}} \quad (2.47)$$

If the use is necessary, then the stiffener is defined following the constraints in Equations 2.48, 2.49, 2.50 and 2.51.

$$b_{sl} \geq 5 + \frac{h_v}{30[cm]} \quad (2.48)$$

$$b_{sl} \geq \frac{b_s}{4} \quad (2.49)$$

$$t_{sl} \geq \frac{b_{sl}}{16} \quad (2.50)$$

$$tw \geq \frac{h_v}{340} \quad (2.51)$$

#### **d) Other verifications**

The slab and girder maximum deflection, slab shear, shear connectors and diaphragms are calculated in the same way as in the Allowable Stress methodology.

## 2.2 Structural Analysis

There are different structural analyses techniques available to bridge engineers accomplish the structural design. They vary from simple code recommendations to more complex procedures. Usually, this choice is based on the engineer preference and his experience.

For instance, AASHTO (2012) suggests the application of simplified formulas when the structure is inside predetermined intervals. Nevertheless, whether these conditions are not valid it is recommended, for example, the application of the Level Rule, which will be explained in Section 2.2.1.

In addition, other structural analyses' simplified procedures common for bridge engineers are the Engesser-Courbon, the Leonhardt and the Fauchart approaches. The first considers that the girders are connected through a rigid beam, while the second takes into account the grid effect. The Fauchart Method is adopted in the present dissertation. Differently from the previous schemes, it does not consider the existence of beams connecting the bridge girders. More details on this approach will be given in Section 2.2.1.

A more refined model to determine the stress distribution on the structure can be constructed using the Finite Element Method (FEM). Despite it being a more complex methodology, requiring a careful engineering interpretation, it is expected to achieve more precise results. This method, also used in this dissertation, is described in Section 2.2.2.

### 2.2.1 Simplified Models

The simplified static models are usually employed by bridge designers. The deck stresses are found using Rüschi's tables (RÜSCH, 1965), which are added to the Annex. To determine the load in girders originated from the vehicle model many different methodologies can be applied. This dissertation will use the conventional Level Rule and the Fauchart model, both described below.

#### **a) Level Rule (LR)**

The level rule is used by many designers, being the most simplified way to determine the girders loads. This method was chosen because it is applicable in all situations, not being limited by the range of applicability of AASHTO approximate formulas, and was the one used

in the comparison example (Pinho & Bellei (2007)) of Chapter 5. It assumes that the deck in its transverse direction is simply supported by the girders and uses static to determine the reaction force to be applied in the girder. Figures 7 and 8 demonstrate an example of the level rule application to find the stresses on the second beam.

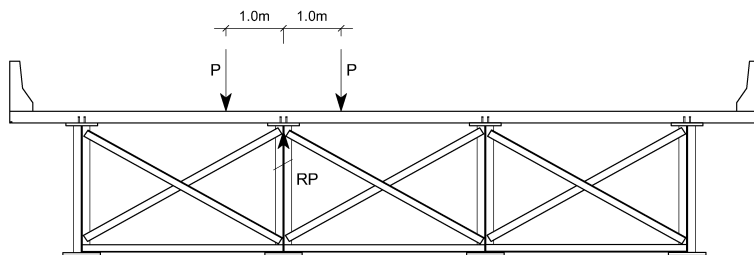


Figure 7 – Level rule for the tire load

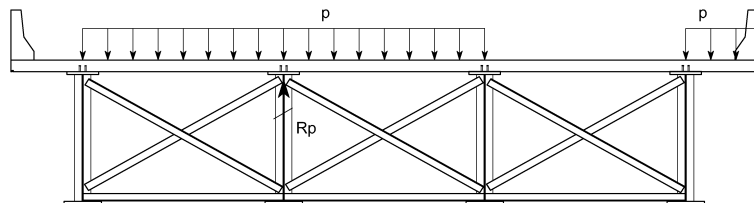


Figure 8 – Level rule for the uniform loading

Then, after this step these reaction forces are applied in the actual simply supported girder to determine the bending moment and shear stress of the structure.

### b) Fauchart Model (FM)

According to Stucchi (2006) and Moura et al. (2016) the rigid deck premise cannot be a good approximation to bridges with a reduced number of cross-beams or when it is employed diaphragms. In these cases, they recommend the use of the Fauchart Method.

In this approach, it is disregarded the slab longitudinal flexibility. Moreover, the Euler-Bernoulli beam model is valid to girders, which

are considered self-supported and with constant moment of inertia.

From that, the first equations can be drawn. Equation 2.52 states that the girder element alone have to obey the differential equation of the elastic line:

$$\frac{d^4w}{dx^4} = \frac{p(x)}{EI_y} \quad (2.52)$$

where  $w$  is the vertical displacement in each  $x$  point;  $E$  is the elastic modulus;  $I_y$  is the cross sectional inertia;  $p(x)$  is the uniform loading.

The girder also is governed by the torsion differential equation (Equation 2.53):

$$\frac{d^2\theta}{dx^2} = \frac{m(x)}{GJ_t} \quad (2.53)$$

where  $\theta$  is the torsion angle in each  $x$  point;  $G$  is the shear modulus;  $J_t$  is the torsional inertia;  $m(x)$  is the uniform distributed torsion moment.

Using the Fourier series, these differential equations are transformed in algebraic equations. After all the mathematical manipulations it results in Equations 2.54 and 2.55.

$$k_v = EI_y \left( \frac{\pi}{L_b} \right)^4 \quad (2.54)$$

$$k_t = GJ_t \left( \frac{\pi}{L_b} \right)^2 \quad (2.55)$$

where  $k_v$  and  $k_t$  are the vertical and torsional spring constants, respectively.

Those spring constants are used in the structure model, representing the girders in the bridge cross section (Figure 9).

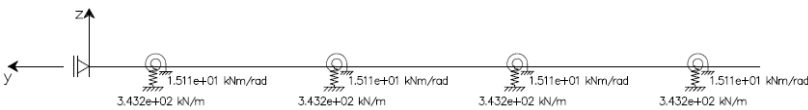


Figure 9 – Fauchart Model

From this model it is possible to obtain the influence lines and the resultant forces for each load configuration.

### 2.2.2 Finite Element Model (FEM)

It was developed an in-house Matlab FEM code to represent the bridge structure. For further details on this subject, the reader is referred to Ferreira (2008) and Vaz (2011) and the references therein.

The girders are modeled using a 2-node, 6-DOF, Euler-Bernoulli frame element. The bridge deck is represented through a 4-node rectangular shell element. It is a composition of a membrane and a plate element. The eccentricity between the slab mid-surface and the beam axis is considered by introducing a rigid link.

This section describes the methodology used for each element of the model.

#### a) Frame Element

The girders are modeled using a 2-node, 6-DOF per node (3 translations and 3 rotations), Euler-Bernoulli frame element. It is employed linear polynomials to represent longitudinal displacements  $u(x)$  and torsion rotations  $\theta_x(x)$  whereas cubic polynomials to describe the transversal displacements  $v(x)$  and  $w(x)$ , as shown in Equations 2.56 and 2.57:

$$\begin{cases} u(x) = \alpha_1 + \alpha_2 x \\ \theta_x(x) = \alpha_1 + \alpha_2 x \end{cases} \quad (2.56)$$

$$\begin{cases} v(x) = \alpha_3 + \alpha_4 x + \alpha_5 x^2 + \alpha_6 x^3 \\ w(x) = \alpha_3 + \alpha_4 x + \alpha_5 x^2 + \alpha_6 x^3 \\ \frac{dv(x)}{dx} = \theta_z(x) \\ \frac{dw(x)}{dx} = \theta_y(x) \end{cases} \quad (2.57)$$

where  $u(x)$ ,  $\theta_x(x)$ ,  $v(x)$ ,  $w(x)$ ,  $\theta_z(x)$  and  $\theta_y(x)$  are the displacements function;  $\alpha_i$  for  $i = 1..6$  are the polynomial parameters.

It is convenient to write the polynomial parameters  $\alpha_i$  as function of the nodal displacements and rotations. To solve these Equations, first consider a beam element with length  $L$  and DOFs (Equation 2.58) as shown in Figure 10.

$$\mathbf{d}^T = \{d_1 \ d_2 \ \dots \ d_{12}\} = \{u_1 \ v_1 \ w_1 \ \theta_{x1} \ \theta_{y1} \ \theta_{z1} \ u_2 \ v_2 \ w_2 \ \theta_{x2} \ \theta_{y2} \ \theta_{z2}\} \quad (2.58)$$

where  $\mathbf{d}^T$  is the transpose vector of nodal DOFs;  $u_i$ ,  $v_i$  and  $w_i$  are the translations in direction x, y and z respectively;  $\theta_{xi}$ ,  $\theta_{yi}$  and  $\theta_{zi}$  are the rotations around the x, y and z axis, respectively.

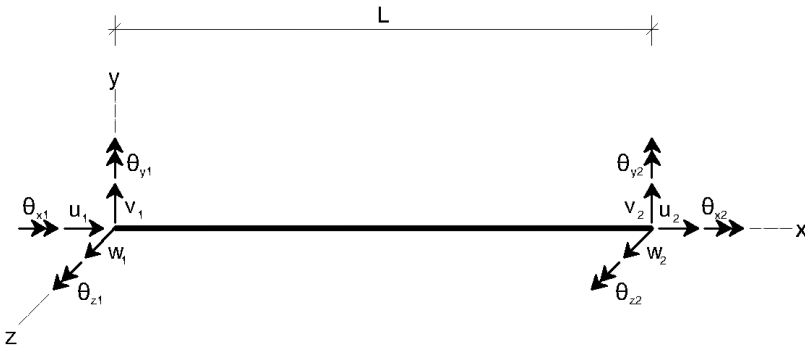


Figure 10 – Beam element

Then, applying the boundary conditions the beam shape functions will result. These shape functions will constitute the matrix  $\mathbf{N}$  for the general MEF formulation. Therefore, the displacements can be expressed as indicated by Equation 2.59.

$$\mathbf{u} = \mathbf{N}\mathbf{d} \quad (2.59)$$

where  $\mathbf{u}$  is the displacements vector;  $\mathbf{N}$  is the matrix of shape functions.



Then, the strain can be obtained from Equation 2.59, making the derivative of matrix  $\mathbf{N}$  in  $x$ . It results in Equation 2.60.

$$\boldsymbol{\varepsilon} = \mathbf{L}\mathbf{u} = \mathbf{L}\mathbf{N}\mathbf{d} = \mathbf{B}\mathbf{d} \quad (2.60)$$

where  $\boldsymbol{\varepsilon}$  is the strain vector;  $\mathbf{L}$  is the matrix containing the differential operators;  $\mathbf{B}$  is the strain-displacement matrix, that contains the spatial derivatives of the  $x$  variable.

The stresses in the element are obtained through the Hooke's Law (Equation 2.61).

$$\boldsymbol{\sigma} = \mathbf{C}\boldsymbol{\varepsilon} \quad (2.61)$$

where  $\boldsymbol{\sigma}$  is the stress vector;  $\mathbf{C}$  is the matrix of constitutive relations, which for an isotropic material depends only of:  $E$ , elastic modulus and  $\nu$ , Poisson coefficient.

Therefore, using the matrices  $\mathbf{N}$ ,  $\mathbf{B}$  and  $\mathbf{C}$  and applying the Principle of Virtual Work (Equation 2.62), the stiffness matrix  $\mathbf{K}$  and the equivalent nodal forces vector  $\mathbf{f}$  are determined.

$$\int_0^V \boldsymbol{\delta}\boldsymbol{\varepsilon}^t \boldsymbol{\sigma} dV = \int_0^V \boldsymbol{\delta}\mathbf{u}^t \mathbf{q} dV + \int_0^\Gamma \boldsymbol{\delta}\mathbf{u}^t \mathbf{p} d\Gamma + \boldsymbol{\delta}\mathbf{d}^t \mathbf{f} \quad (2.62)$$

where  $\mathbf{q}$ ,  $\mathbf{p}$  and  $\mathbf{f}$  are the body forces, the surface tractions and the nodal forces vectors, respectively;  $\boldsymbol{\delta}\boldsymbol{\varepsilon}$  is the virtual strain vector;  $\boldsymbol{\delta}\mathbf{u}$  is the virtual displacement vector;  $\boldsymbol{\delta}\mathbf{d}$  is the virtual nodal displacements vector.

The virtual strain vector and the virtual displacement vector can be written according to Equations 2.63 and 2.64.

$$\boldsymbol{\delta}\mathbf{u} = \mathbf{N}\boldsymbol{\delta}\mathbf{d} \quad (2.63)$$

$$\boldsymbol{\delta}\boldsymbol{\varepsilon} = \mathbf{B}\boldsymbol{\delta}\mathbf{d} \quad (2.64)$$

Thus, substituting these expressions and the Equations 2.59, 2.60 and 2.61 in Equation 2.62, it is found the Equation 2.65.

$$\delta \mathbf{d}^t \int_0^V \mathbf{B}^t \mathbf{C} \mathbf{B} dV \mathbf{d} = \delta \mathbf{d}^t \left( \int_0^V \mathbf{N}^t \mathbf{q} dV + \int_0^\Gamma \mathbf{N}^t \mathbf{p} d\Gamma + \mathbf{f} \right) \quad (2.65)$$

Because the virtual nodal displacements vector is arbitrary, it may be eliminated, resulting in Equation 2.66.

$$\mathbf{K} \mathbf{d} = \mathbf{f}_q + \mathbf{f}_p + \mathbf{f} \quad (2.66)$$

where  $\mathbf{f}_q$ ,  $\mathbf{f}_p$  are the equivalent nodal forces vector corresponding to the body and surface tractions while  $\mathbf{f}$  is the nodal forces vector itself.

The stiffness matrices and force vectors of each element are combined adequately to properly form the structure global matrix  $\mathbf{K}_g$  and vector  $\mathbf{f}_g$ .

Finally, it is added the eccentricity between the slab mid-surface and the beam axis consideration by introducing a rigid link (COOK et al., 2007), as shown in Figure 11 and Equation 2.67.

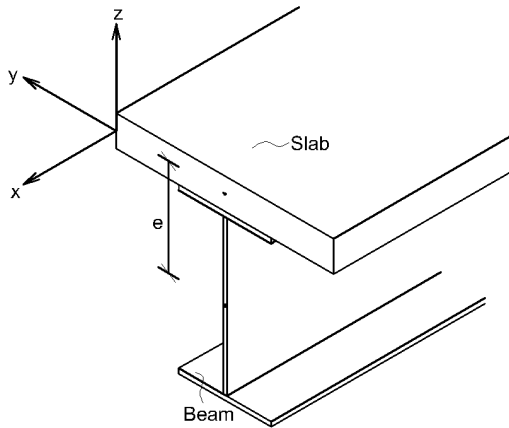


Figure 11 – Eccentricity between slab and beam axis

$$\begin{Bmatrix} u_{xb} \\ u_{zb} \\ \theta_{yb} \end{Bmatrix} = \mathbf{T}_B \begin{Bmatrix} u_{xp} \\ u_{zp} \\ \theta_{yp} \end{Bmatrix} \quad (2.67)$$

$$\mathbf{T}_B = \begin{bmatrix} 1 & 0 & -e \\ 0 & 1 & 0 \\ 0 & 0 & 1 \end{bmatrix} \quad (2.68)$$

where  $u_{xb}$  is the beam nodal displacement in x;  $u_{zb}$  is the beam nodal displacement in z;  $\theta_{yb}$  is the beam nodal rotation around y;  $u_{xp}$  is the plate nodal displacement in x;  $u_{zp}$  is the plate nodal displacement in z;  $\theta_{yp}$  is the plate nodal rotation around y;  $\mathbf{T}_B$  is the transformation matrix relating the beam nodal displacements and rotations with the shell nodal displacements and rotations;  $e$  is the eccentricity between slab and beam axis.

### b) Shell Element

The bridge deck is represented by a 4-node rectangular shell element. It is a composition of a membrane and a plate element. The plate is designed by the Mindlin theory, which makes the following considerations:

- a normal to the shell mid-section, straight line keeps being straight after the forces application. However, it does not necessarily keep being perpendicular to the surface;
- there is only vertical displacements,  $w(x, y, z)$ ;
- the strain,  $\varepsilon_z$ , is zero at any plate point.

The plate displacements are defined by Equation 2.69. From that, the strain matrix (Equation 2.70) can be deduced and simplified by

Equation 2.71.

$$\begin{cases} u(x, y, z) = z\theta_y \\ v(x, y, z) = -z\theta_x \\ w(x, y, z) = 0 \end{cases} \quad (2.69)$$

$$\begin{Bmatrix} \varepsilon_x \\ \varepsilon_y \\ \lambda_{xy} \\ \lambda_{yz} \\ \lambda_{xz} \end{Bmatrix} = \begin{bmatrix} z & 0 & 0 & 0 & 0 \\ 0 & z & 0 & 0 & 0 \\ 0 & 0 & z & 0 & 0 \\ 0 & 0 & 0 & 1 & 0 \\ 0 & 0 & 0 & 0 & 1 \end{bmatrix} \begin{Bmatrix} \theta_{y,x} \\ -\theta_{x,y} \\ \theta_{y,y} - \theta_{x,x} \\ w_{,y} - \theta_x \\ w_{,x} + \theta_y \end{Bmatrix} \quad (2.70)$$

$$\begin{Bmatrix} \varepsilon_b \\ \varepsilon_s \end{Bmatrix} = \mathbf{T}_M \mathbf{k}_M = \begin{bmatrix} \mathbf{T}_b & \mathbf{0} \\ \mathbf{0} & \mathbf{T}_s \end{bmatrix} \begin{Bmatrix} \mathbf{k}_b \\ \mathbf{k}_s \end{Bmatrix} \quad (2.71)$$

where  $u$ ,  $v$  and  $w$  are the displacements in the x, y and z directions, respectively;  $\theta_x$  and  $\theta_y$  are the rotations around the x and y axis, respectively;  $\varepsilon_x$  and  $\varepsilon_y$  are the strains in the directions indicated by the index;  $\lambda_{xy}$ ,  $\lambda_{yz}$  and  $\lambda_{xz}$  are the transverse shear deformations in the plane indicated by the index;  $\varepsilon_b$  and  $\varepsilon_s$  represents the vector of strains and shear deformations;  $\mathbf{T}_M$  is the Mindlin transformation matrix, subdivided in  $\mathbf{T}_b$  and  $\mathbf{T}_s$ ;  $\mathbf{k}_M$  is the Mindlin curvature and transverse shear strain vector, subdivided in  $\mathbf{k}_b$  and  $\mathbf{k}_s$ .

To continue the deductions of the finite element it is chosen to use the isoparametric element of the Serendipity family. A isoparametric element uses the same shape functions for kinematic purposes and for geometric measurements. Thus, the field that describes the Cartesian coordinates of a quadrilateral element must be a 4<sup>th</sup> term polynomial with parametric coordinates (Figure 12 and Equation 2.72 or, in short, Equation 2.73 ).

$$\begin{cases} u(\xi, \eta) = a_1 + a_2\xi + a_3\eta + a_4\xi\eta \\ v(\xi, \eta) = a_5 + a_6\xi + a_7\eta + a_8\xi\eta \end{cases} \quad (2.72)$$

$$\mathbf{u}(\xi, \eta) = \mathbf{N}\mathbf{a}(\xi, \eta)\mathbf{a} \quad (2.73)$$

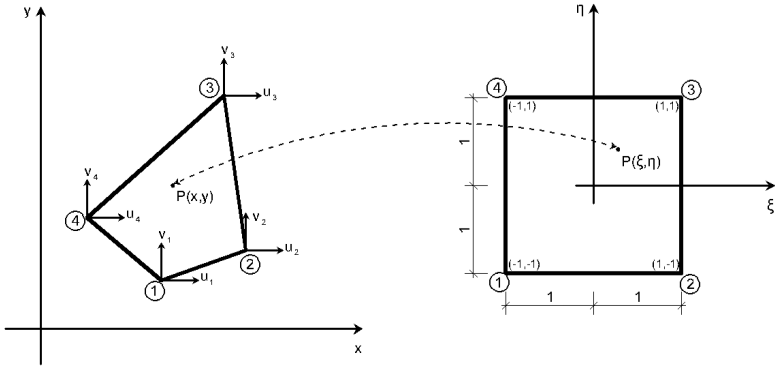


Figure 12 – Quadrilateral element of the Serendipity family

where  $u(\xi, \eta)$  and  $v(\xi, \eta)$  are the parametric displacements and  $\mathbf{u}(\xi, \eta)$  is the parametric displacements vector;  $a_i$  with  $i = 1, \dots, 8$  are the polynomial parameters and  $\mathbf{a}$  is its vector notation;  $\xi$  and  $\eta$  are the parametric coordinates, which can be represented by matrix  $\mathbf{N}\mathbf{a}(\xi, \eta)$ .

From Figure 12 it is possible to deduce the boundary conditions, which leads to Equation 2.74 or, succinctly, Equation 2.75.

$$\begin{Bmatrix} u_1 \\ v_1 \\ u_2 \\ v_2 \\ u_3 \\ v_3 \\ u_4 \\ v_4 \end{Bmatrix} = \begin{bmatrix} 1 & -1 & -1 & 1 & 0 & 0 & 0 & 0 \\ 0 & 0 & 0 & 0 & 1 & -1 & -1 & 1 \\ 1 & 1 & -1 & -1 & 0 & 0 & 0 & 0 \\ 0 & 0 & 0 & 0 & 1 & 1 & -1 & -1 \\ 1 & 1 & 1 & 1 & 0 & 0 & 0 & 0 \\ 0 & 0 & 0 & 0 & 1 & 1 & 1 & 1 \\ 1 & -1 & 1 & -1 & 0 & 0 & 0 & 0 \\ 0 & 0 & 0 & 0 & 1 & -1 & 1 & -1 \end{bmatrix} \begin{Bmatrix} a_1 \\ a_2 \\ a_3 \\ a_4 \\ a_5 \\ a_6 \\ a_7 \\ a_8 \end{Bmatrix} \quad (2.74)$$

$$\mathbf{d} = \mathbf{A}\mathbf{a} \quad (2.75)$$

where  $\mathbf{d}$  is the nodal DOF.

Substituting Equation 2.75 on Equation 2.73 it results in:

$$\mathbf{u}(\xi, \eta) = \mathbf{N}\mathbf{a}(\xi, \eta)\mathbf{A}^{-1}\mathbf{d} \quad (2.76)$$

Considering,

$$\mathbf{N}(\xi, \eta) = \mathbf{N}\mathbf{a}(\xi, \eta)\mathbf{A}^{-1} \quad (2.77)$$

the Equation 2.76 can be written as,

$$\mathbf{u}(\xi, \eta) = \mathbf{N}(\xi, \eta)\mathbf{d} \quad (2.78)$$

where matrix  $\mathbf{N}(\xi, \eta)$  is composed by the shape functions and is defined by Equation 2.79.

$$\mathbf{N}(\xi, \eta) = \begin{bmatrix} N_1(\xi, \eta) & 0 & N_2(\xi, \eta) & 0 & N_3(\xi, \eta) & 0 & N_4(\xi, \eta) & 0 \\ 0 & N_1(\xi, \eta) & 0 & N_2(\xi, \eta) & 0 & N_3(\xi, \eta) & 0 & N_4(\xi, \eta) \end{bmatrix} \quad (2.79)$$

Using Equations 2.79 and 2.78 the displacements can be written as Equation 2.80 and, analogously, the coordinates as Equation 2.81.

$$\begin{cases} u(\xi, \eta) = \sum_{i=1}^4 N_i(\xi, \eta)u_i \\ v(\xi, \eta) = \sum_{i=1}^4 N_i(\xi, \eta)v_i \end{cases} \quad (2.80)$$

$$\begin{cases} x(\xi, \eta) = \sum_{i=1}^4 N_i(\xi, \eta)x_i \\ y(\xi, \eta) = \sum_{i=1}^4 N_i(\xi, \eta)y_i \end{cases} \quad (2.81)$$

The shape functions  $N_i(\xi, \eta)$  are defined by Equation 2.82

$$\begin{cases} N_1(\xi, \eta) = \frac{1}{4}(1 - \xi)(1 - \eta) \\ N_2(\xi, \eta) = \frac{1}{4}(1 + \xi)(1 - \eta) \\ N_3(\xi, \eta) = \frac{1}{4}(1 + \xi)(1 + \eta) \\ N_4(\xi, \eta) = \frac{1}{4}(1 - \xi)(1 + \eta) \end{cases} \quad (2.82)$$

However, when the Serendipity element is brought to use with the Mindlin theory, it is necessary to change the displacements field from Equation 2.80 to consider the rotations  $\theta_x(x, y)$  and  $\theta_y(x, y)$  as well as the z-axis displacement  $w(x, y)$ . The new displacements field is shown in Equation 2.83 and Figure 13.

$$\begin{cases} w(\xi, \eta) = \sum_{i=1}^{nnos} N_i(\xi, \eta)w_i \\ \theta_x(\xi, \eta) = \sum_{i=1}^{nnos} N_i(\xi, \eta)\theta_{x_i} \\ \theta_y(\xi, \eta) = \sum_{i=1}^{nnos} N_i(\xi, \eta)\theta_{y_i} \end{cases} \quad (2.83)$$

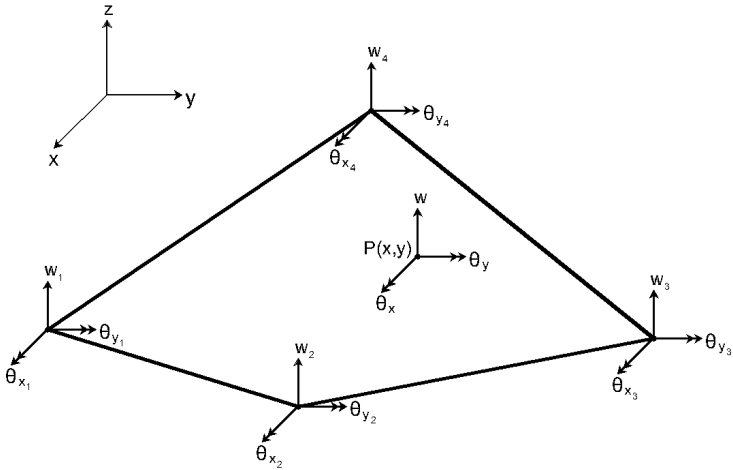


Figure 13 – Quadrilateral element of the Serendipity family by the Mindlin theory

Considering Equations 2.71 and 2.83, the sub-vectors  $\mathbf{k}_b$  and  $\mathbf{k}_s$  can be defined as Equations 2.84 and 2.85 or 2.86 and 2.87, succinctly.

$$\mathbf{k}_b(\xi, \eta) = \sum_{i=1}^{nnos} \begin{bmatrix} 0 & 0 & N_i(\xi, \eta)_{,x} \\ 0 & -N_i(\xi, \eta)_{,y} & 0 \\ 0 & -N_i(\xi, \eta)_{,x} & N_i(\xi, \eta)_{,y} \end{bmatrix} \begin{Bmatrix} w_i \\ \theta_{x_i} \\ \theta_{y_i} \end{Bmatrix} \quad (2.84)$$

$$\mathbf{k}_s(\xi, \eta) = \sum_{i=1}^{n_{nos}} \begin{bmatrix} N_i(\xi, \eta)_{,x} & 0 & N_i(\xi, \eta) \\ N_i(\xi, \eta)_{,y} & -N_i(\xi, \eta) & 0 \end{bmatrix} \begin{Bmatrix} w_i \\ \theta_{x_i} \\ \theta_{y_i} \end{Bmatrix} \quad (2.85)$$

$$\mathbf{k}_b(\xi, \eta) = \mathbf{B}_b(\xi, \eta) \mathbf{d} \quad (2.86)$$

$$\mathbf{k}_s(\xi, \eta) = \mathbf{B}_s(\xi, \eta) \mathbf{d} \quad (2.87)$$

where  $\mathbf{B}_b$  is the bending strain-displacement matrix;  $\mathbf{B}_s$  is the transverse shear strain-displacement matrix.

Using Equations 2.86 and 2.87 the compatibility Equation 2.71 can be rewritten as:

$$\begin{cases} \boldsymbol{\varepsilon}_b(\xi, \eta, z) = z \mathbf{B}_b(\xi, \eta) \mathbf{d} \\ \boldsymbol{\varepsilon}_s(\xi, \eta) = \mathbf{B}_s(\xi, \eta) \mathbf{d} \end{cases} \quad (2.88)$$

Considering those Equations and the Hooke Law, Equation 2.89 is obtained.

$$\begin{cases} \boldsymbol{\sigma}_b(\xi, \eta, z) = z \mathbf{C}_b \mathbf{B}_b(\xi, \eta) \mathbf{d} \\ \boldsymbol{\sigma}_s(\xi, \eta) = \mathbf{C}_s \mathbf{B}_s(\xi, \eta) \mathbf{d} \end{cases} \quad (2.89)$$

where  $\mathbf{C}_b$  is the bending constitutive matrix;  $\mathbf{C}_s$  is the transverse shear constitutive matrix.

Then, using the Principle of Virtual Work it is possible to obtain the stiffness matrix. For that, the virtual strains will be:

$$\begin{cases} \boldsymbol{\delta \varepsilon}_b(\xi, \eta, z) = z \mathbf{B}_b(\xi, \eta) \boldsymbol{\delta d} \\ \boldsymbol{\delta \varepsilon}_s(\xi, \eta) = \mathbf{B}_s(\xi, \eta) \boldsymbol{\delta d} \end{cases} \quad (2.90)$$

where  $\boldsymbol{\delta \varepsilon}_b(\xi, \eta, z)$  is the bending virtual strain vector;  $\boldsymbol{\delta \varepsilon}_s(\xi, \eta)$  is the transversal shear virtual strain vector;  $\boldsymbol{\delta d}$  is the vector of virtual nodal DOF.



Applying the Principle of Virtual Work separately for bending and shear it is obtained:

$$\int_V \delta \varepsilon_b^t \sigma_b dv + \int_V \delta \varepsilon_s^t \sigma_s dv = \delta \mathbf{d}^t \mathbf{f} \quad (2.91)$$

$$\begin{aligned} \delta \mathbf{d}^t \left( \int_A \mathbf{B}_b(\xi, \eta)^t \int_{-\frac{t}{2}}^{\frac{t}{2}} z^2 \mathbf{C}_b dt \mathbf{B}_b(\xi, \eta) dA \right. \\ \left. + \int_A \mathbf{B}_s(\xi, \eta)^t \int_{-\frac{t}{2}}^{\frac{t}{2}} \mathbf{C}_s dt \mathbf{B}_s(\xi, \eta) dA \right) \mathbf{d} = \delta \mathbf{d}^t \mathbf{f} \end{aligned} \quad (2.92)$$

where the integrals in  $V$  and  $A$  are volume and area integrals;  $t$  is the plate height;  $\mathbf{f}$  is the forces vector.

As  $\delta \mathbf{d}$  is arbitrary, it can be eliminated from Equation 2.92. Considering that  $\mathbf{D}_b = \frac{t^3}{12} \mathbf{C}_b$  and  $\mathbf{D}_s = t \mathbf{C}_s$  and integrating in the height, it results in:

$$\left( \int_A \mathbf{B}_b(\xi, \eta)^t \mathbf{D}_b \mathbf{B}_b(\xi, \eta) dA + \int_A \mathbf{B}_s(\xi, \eta)^t \mathbf{D}_s \mathbf{B}_s(\xi, \eta) dA \right) \mathbf{d} = \mathbf{f} \quad (2.93)$$

Or, in short:

$$(\mathbf{K}_b + \mathbf{K}_s) \mathbf{d} = \mathbf{f} \quad (2.94)$$

where  $\mathbf{K}_b$  is the plate bending stiffness matrix;  $\mathbf{K}_s$  is the plate transverse shear stiffness matrix.

It is important to highlight that, as  $\mathbf{B}_b$  and  $\mathbf{B}_s$  are functions of parametric variables  $\xi$  and  $\eta$ , the integrations of Equation 2.93 will be made using the Gaussian quadrature.

The plate stiffness matrix is, then, found combining both the bending and transverse shear stiffness matrices, as shown in Equation 2.95.

$$\mathbf{K}_p = \begin{bmatrix} \mathbf{K}_b & \mathbf{0} \\ \mathbf{0} & \mathbf{K}_s \end{bmatrix} \quad (2.95)$$

The membrane element follows the same deduction logic as the plate, however it is modelled considering the plane displacements  $u_i$  and  $v_i$ . Then, to obtain the shell element matrix, the membrane and plate elements are combined in Equation 2.96. For the final element the rotation around the slab perpendicular axis is disregarded.

$$\mathbf{K}_{shell} = \begin{bmatrix} \mathbf{K}_m & \mathbf{0} \\ \mathbf{0} & \mathbf{K}_p \end{bmatrix} \quad (2.96)$$

where  $\mathbf{K}_{shell}$  is the shell stiffness matrix (20x20);  $\mathbf{K}_m$  is the membrane stiffness matrix (8x8);  $\mathbf{K}_p$  is the plate stiffness matrix (12x12).

## Chapter 3

# Fundamentals of Optimization

This chapter describes an overview on engineering optimization. Firstly, general concepts of optimization are shown. Then, the heuristic algorithms employed in this dissertation are detailed. Finally, the statistic tests used to compare the efficiency between algorithms are explained. For further details on the matter, the reader is referred to Arora (2004), Civicioglu (2013), Yang (2010), Holland (1975), Atashpaz-Gargari & Lucas (2007), Gonçalves, Lopez & Miguel (2015), Schervish (2012) and the references therein.

### 3.1 General Concepts

The practical use of optimization processes begins with the definition of, at least, one objective, which is the performance mode that the system will be analyzed. It can be, for example, a structure cost minimization. This objective is dependent of certain system characteristics, which are called design variables. The optimization goal is to find the design variable values that give the best value for the objective. Sometimes these variables are limited to certain values which results in a restricted optimization problem. Thereby, an optimization problem can be divided in the following elements:

- Objective function: function associated with the analyzed system

parameters and used to measure its performance. Mathematically it can be described as the function  $J$  proving the system performance value associated with  $n$  parameters with real values. As an example it can be considered the concrete volume of a bridge beam;

- Design variables: parameters that define the system, which can be modified by the designer to improve its performance. In mathematics, it can be considered the vector  $\mathbf{x} = (x_1, \dots, x_n)$  with  $n$  real adjustable parameters. This value is associated with the region  $V$ . In the previous example, the design variables  $x_1$  and  $x_2$  can be the height and width of the beam cross section, respectively;
- Restrictions: limitations to the designers choices. In general, it is a not empty sub-domain of  $V$ , here called  $S$ . In the beam problem a relation between design variables can be imposed, such as  $0,5 \leq \frac{x_2}{x_1} \leq 1,0$ .

Then, an optimization problem can be described as Equation 3.1.

$$x^* = \operatorname{argmin}\{J(x) : x \in S\} \quad (3.1)$$

where  $J$  is the function to be minimized;  $x$  are the design variables;  $S = \{g_j(x) \leq 0, 1 \leq i \leq n_c, h_j(x) = 0, 1 \leq j \leq n_e\}$  is the project admissible region,  $g_j$  and  $h_j$  are the inequality and equality restrictions, respectively.

The problem consists in identifying the  $J$  global minimum, finding a  $x^* \in S$  that  $J(x^*) \leq J(x) \forall x \in S$ . Note that if neither the  $J$  nor the  $S$  are convex there can be a local minimum,  $x^* \in S$  that  $J(x^*) \leq J(x) \forall x \in S / \|x - x^*\| \leq \varepsilon, \varepsilon > 0$ .

In general situations there can be many local and global minimums. Figure 14 shows an example of an one variable function with two local minimums and only one global minimum. Between the minimums, the one with the smaller value of  $J$  is the global minimum.

It is important to highlight that, generally, optimization algorithms are iterative. They begin with a design variable initial value

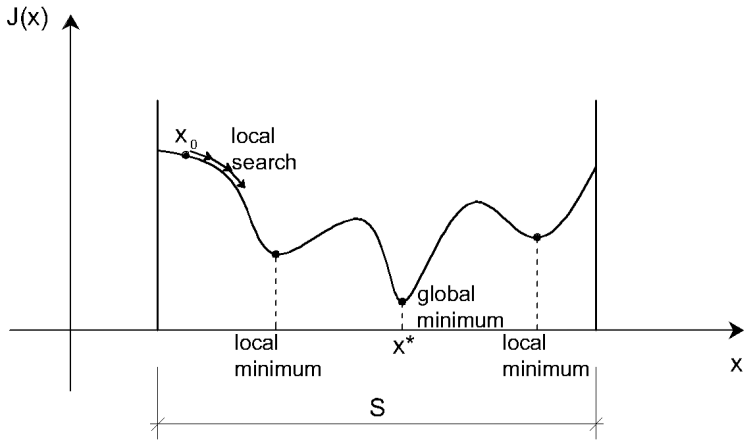


Figure 14 – Local and global minimum

$x_0$  and generate a sequence of points  $(x_0, x_1, \dots, x_{nit})$  that, supposedly, will converge to the problem solution. The strategy used to move from one point to another is the difference between the many optimization algorithms. The mathematical methods, usually, use the values of the objective function and restrictions, besides its first and second derivatives. However, the disadvantage of those methods is to demand too many problem data. In structural problems, the optimization function does not necessarily have derivatives and it is even less likely to prove its convexity.

Therefore, when there is a complex problem to be solved, optimization heuristic algorithms are used. These have a computational cost higher than the mathematical methods, but are capable of finding solutions for any problem. Besides that, the mathematical methods will only find solutions with continuous variables. Thus, when the use of discrete variables is necessary, it is opted to solve the problem with a heuristic algorithm. Section 3.2 will describe the algorithms used in this work.

## 3.2 Algorithms

The algorithms used in this study are well known optimization heuristic algorithms: Backtracking Search Algorithm (BSA), Firefly Algorithm (FA), Genetic Algorithm (GA), Imperialist Competitive Algorithm (ICA) and Search Group Algorithm (SGA). The operation of each one will be detailed in the next subsections.

### 3.2.1 Backtracking Search Algorithm (BSA)

The Backtracking Search Algorithm (BSA) is an evolutionary algorithm created by Civicioglu (2013). It is a population based iterative algorithm divided into five processes: Initialization, Selection-I, Mutation, Crossover and Selection-II.

Algorithm 1 shows the BSA general structure.

---

#### Algorithm 1 General Structure of BSA

---

```

procedure BSA
  Initialization
  loop:
  Selection-I
  Mutation
  Crossover
  Slection-II
  go to loop until stopping conditions are met
end

```

---

After the initialization of the population, the Selection-I stage determines the historical population of the algorithm. Then, the Mutation generates a new population, which is based on the results of the two previous stages, as shown in Equation 3.2,

$$Mutant = Pop + F(oldP - P) \quad (3.2)$$

where  $Pop$  is the population created in the Initialization process;  $oldP$  is the historical population;  $F$  is a random value to control the amplitude of  $(oldP - P)$ .

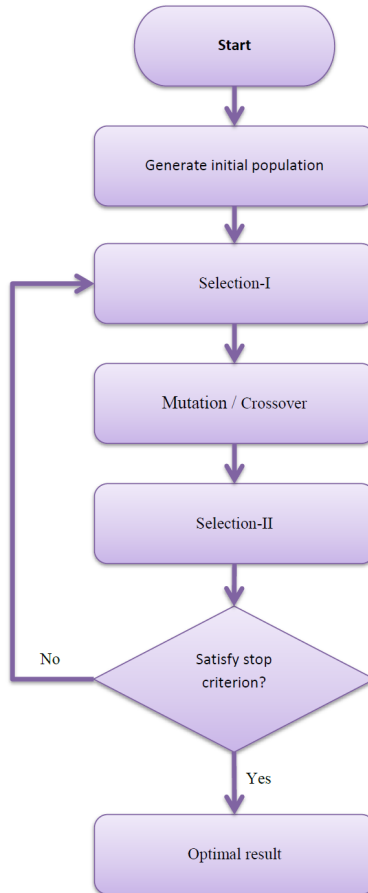


Figure 15 – BSA flowchart

The Crossover phase generates the final form of the trial population ( $T_i$ ), which will be used in the Selection-II stage. This last operation of the BSA is based on a greedy selection, where the  $T_i$ s that have better fitness values than the corresponding  $P_i$ s are used to update the  $P_i$ s.

### 3.2.2 Firefly Algorithm (FA)

The Firefly Algorithm (FA) is a meta-heuristic algorithm developed by Yang (2010) and it is based on the flashing patterns and behavior of fireflies. In this population based algorithm each candidate is modeled as a firefly, which explores the search space randomly while being attracted to brighter fireflies. Its brightness is proportional to the value of the objective function, where the brightest one have the best solution of the problem. Equation 3.3 represents how the firefly  $i$  will be attracted toward the brighter firefly  $j$ :

$$x_i^{it+1} = x_i^{it} + \beta_0 e^{-\gamma r_{ij}^2} (x_j^t - x_i^{it}) + \alpha_r \varepsilon_r^{it} \quad (3.3)$$

where  $\beta_0 \in [0, 1]$  is the attractiveness at  $r = 0$ ;  $r_{ij} = \|x_i - x_j\|_2$  is the Cartesian distance between the two fireflies;  $\varepsilon_r$  is a random vector drawn from a convenient distribution;  $\alpha_r$  is the randomization parameter;  $\gamma$  is the light absorption coefficient, which controls the speed of the convergence.

Algorithm 2 shows the structure of the FA.

---

#### Algorithm 2 General Structure of FA

---

**procedure** FA

*Generate initial population*

*loop:*

*Evaluate fitness*

*Update fitness value*

*Rank the population*

*Update the position*

**go to loop** until stopping conditions are met

**end**

---

### 3.2.3 Genetic Algorithm (GA)

The Genetic Algorithm (GA) is a population based optimization algorithm created by Holland (1975). It uses techniques inspired by the Darwin's Principal of Natural Selection, such as mutation, selection



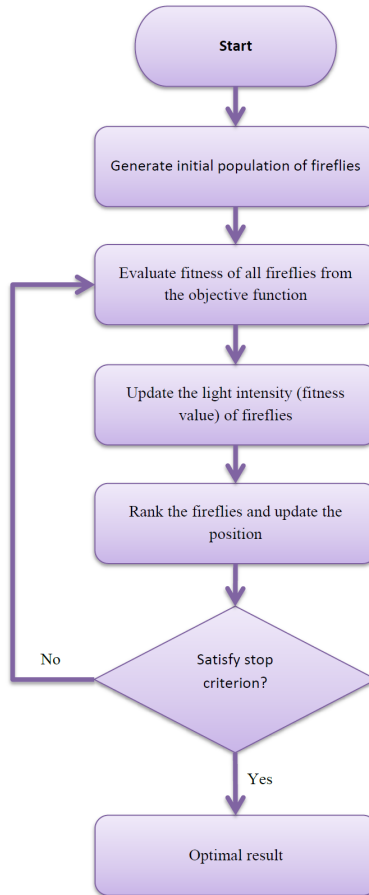


Figure 16 – FA flowchart

and crossover. In this algorithm each member of the population is a chromosome and each variable is a gene of this chromosome.

The selection of the pairs of chromosomes to reproduce the new generation is based on the fitness of the objective function. The fittest chromosome is attributed a greater probability to be chosen. After the selection, the pairs use the crossover operator to get a new offspring and, randomly, a few genes will be mutated.

Algorithm 3 represents the general structure of the GA.

---

**Algorithm 3** General Structure of GA

---

**procedure** GA

*Generate initial population*

*loop:*

*Evaluate fitness*

*Selection*

*Crossover*

*Mutation*

**go to** *loop* until stopping conditions are met

**end**

---

### 3.2.4 Imperialist Competitive Algorithm (ICA)

The Imperialist Competitive Algorithm (ICA) is an evolutionary algorithm developed by Atashpaz-Gargari & Lucas (2007), which uses the imperialistic competition as an inspiration. Its initial population are the countries in the world. Some of the best countries, the ones with the best objective function, are selected to be imperialists and the rest are the colonies of these imperialists.

After forming the empires, the colonies move randomly towards its imperialist. If after this movement any colony is more powerful than its imperialist the colony take its place. The total power of the empires is most affected by the cost of the imperialist as shown in Equation 3.4:

$$T.C._n = Cost(imperialist_n) + \xi_1 mean\{Cost(colonies_n)\} \quad (3.4)$$

where  $T.C._n$  is the total cost of the  $n^{th}$  empire;  $\xi_1$  is a positive number which is considered to be less than 1.

Then the imperialistic competition begins, in which all empires try to take possession of colonies of other empires and control them. When an empire ends up without any colony it is eliminated.

Algorithm 4 shows the flowchart of the ICA.

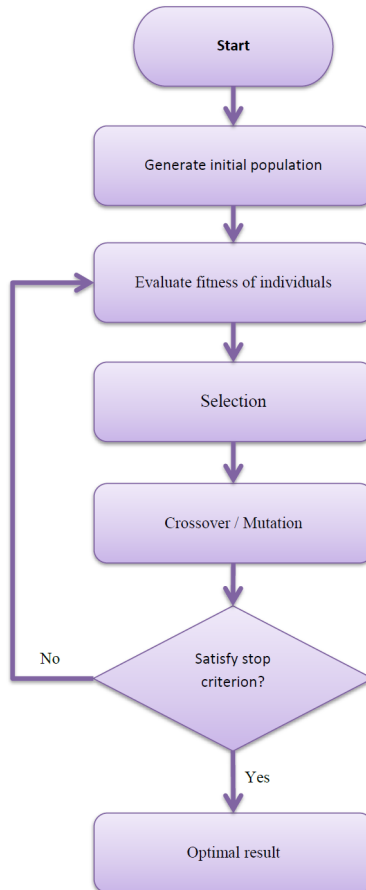


Figure 17 – GA flowchart

### 3.2.5 Search Group Algorithm (SGA)

The Search Group Algorithm (SGA) is a meta-heuristic algorithm developed by Gonçalves, Lopez & Miguel (2015). This algorithm was created to balance the exploration and exploitation phases of an optimum search. It is a population based algorithm divided in two stages (global and local), both containing mutation, generation and selection processes. After the initial population is created and, from these candidates, the

---

**Algorithm 4** General Structure of ICA
 

---

```

procedure ICA
  Initialize the empires
  loop:
  Assimilate colonies
  Revolve some colonies
  if there is a colony with lower cost than its imperialist then
    Exchange the positions of that imperialist and the colony
  end
  Compute the total cost of all empires
  Imperialistic competition
  if there is an is an empire with no colonies then
    Eliminate this empire
    Unite similar empires
  end
  go to loop until stopping conditions are met
end

```

---

initial search groups are chosen the global phase begins.

The choice for the candidate to suffer a mutation is made with the help of an inverse tournament. Then, the generation of the families is the next step of the algorithm. A family is a set of points comprised by one member of the search group and the individuals that it generated. In this process the family members are generated following the Equation 3.5.

$$x_j^{new} = R_{ij} + \alpha_{SGA}\varepsilon_r \quad (3.5)$$

where  $x_j^{new}$  is the perturbed individual;  $R_{ij}$  is the former  $j$ th column of the search group matrix;  $\alpha_{SGA}$  is the parameter that controls the size of the perturbation, which is reduced at each iteration;  $\varepsilon_r$  is a random variable.

The Selection is where lies the difference between the global and the local stages. In the former, it is selected the best candidate of each family to form the next search group, while in the local stage it is chosen the best of all the candidates, without regard of the families.

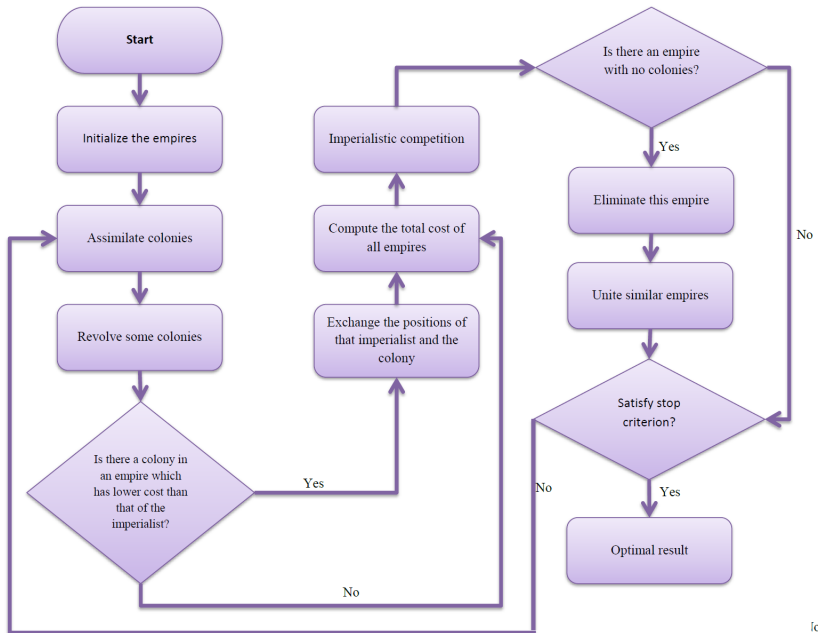


Figure 18 – ICA flowchart

Algorithm 5 shows the structure of the SGA.

### 3.3 Statistic Tests

As it can be noticed by Section 3.2, there are many different methodologies to solve an optimization problem. Then, it is necessary to define comparison criteria between them, to find the one with the best performance for a specific problem. To make this comparison, one can use three criteria:

- Efficiency: identified by the necessary number of objective function evaluations (OFEs) to converge.
- Sturdiness: defined by the algorithm's ability to find the optimum point, independently of the problem configuration and, mainly,

---

**Algorithm 5** General Structure of SGA
 

---

**procedure** SGA*Generate initial population**Evaluate fitness**Form search groups**loop 1:***Global Stage***Mutation**Generate families**Selection***go to** *loop 1* until stopping conditions are met*loop 2:***Local Stage***Mutation**Generate families**Selection***go to** *loop 2* until stopping conditions are met**end**


---

regardless of the initial point.

- Precision: ability to find a specific solution, without being too sensible to data or rounding errors that occur when the algorithm is implemented in a computer.

These three elements are usually in conflict. For example, a method that converges too quickly for a big non-linear problem without restrictions can require too much storage space. On the other hand, a sturdy method can be slower. Compromising between convergence velocity, memory requirements and sturdiness are the central questions of numerical optimization. It is important to highlight that the optimization difficulty lies in the fact that there is no universal algorithm. For combination problems, for example, there is a theorem called "No Free Lunch" (WOLPERT; MACREADY, 1997) that shows that there is no optimum algorithm for all problems. This theorem demonstrates that any optimization method with a good performance for a class of functions can have a bad performance for a different class of problems.

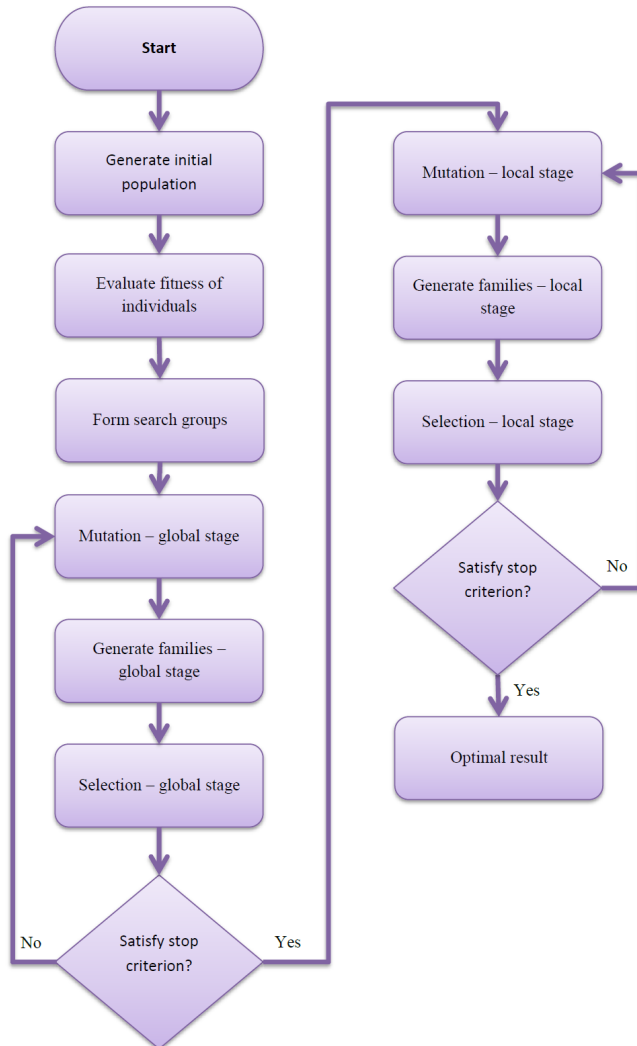


Figure 19 – SGA flowchart

The responsibility to choose the right algorithm lies entirely on the designer. Therefore, this choice is also a very important step, because it frequently determines the quality and velocity of the problem resolution. Thus, one can use statistic tests to help in this choice.

The statistical tests have the purpose of comparing a group of data. That is, in this case, these tests will be used to compare the performance of different optimization algorithms for the solution of the bridge design optimization problem. A very important concept of statistical hypothesis tests is the null hypothesis, i.e. it is the hypothesis that we assume as true for the construction of the test - for more details about this matter the reader is referred to Schervish (2012). Thus, for analyzing the efficiency of the algorithms in this thesis, the null hypothesis can be constructed as: "There is no significant difference between the algorithms". Then, the test will calculate the probability (p-value) of the null hypothesis being correct. If the p-value is too small, less than 0.05 for example, it means that the algorithms are different of each other, i.e. one gives a better performance than the other. However, if the p-value is greater than that, it shows that it is not possible to refute the similarities of the algorithms with only this test.

In the literature there are a lot of types of statistic tests, which will be chosen based on the data type and study form. The data type can be continuous, discrete or binary. In the first one, it is analyzed the continuous results found directly by the algorithm. In this case, it is also necessary to analyze if the results have a normal (parametric) distribution or not (non-parametric). If the results of the optimization are discrete, it shall be used the corresponding test. As for the last type, one can change the optimization results in binary data. For example, if the algorithm reached the problem correct result it is attributed the value 1, otherwise 0. As for the study form, it can be paired if the correct result can be achieved by more than one algorithm or unpaired in the cases that only one of them is capable of such.

Table 1 lists the more usual statistic tests, making the distinction between the data types and study forms that they can be used. Figure 20 demonstrates a chart for choosing the right test in case of continuous data.

---

<sup>1</sup> Known as ANOVA

<sup>2</sup> Also known as Mann-Whitney U test



Table 1 – Statistic Tests

Test	Data	Study	Sample
Fisher's exact test	Binary	Unpaired	2 groups
Chi-square test	Binary	Unpaired	> 2 groups
McNemar test	Binary	Paired	2 groups
Student's t-test	Continuous / Parametric	Paired and Unpaired	2 groups
Analysis of Variance <sup>1</sup>	Continuous / Parametric	Paired and Unpaired	> 2 groups
Wilcoxon's rank sum test <sup>2</sup>	Continuous / Non-Parametric	Paired and Unpaired	2 groups
Kruskal-Wallis test	Continuous / Non-Parametric	Unpaired	> 2 groups
Friedman test	Continuous / Non-Parametric	Paired	> 2 groups

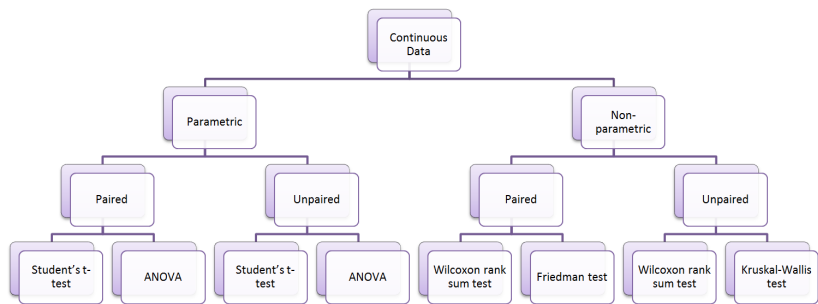


Figure 20 – Statistic Tests

For algorithm comparisons, Whitley et al. (1995) developed test-functions for the optimization of continuous problems. Rojas et al. (2002) made a statistic study of algorithm convergence. This study is based on the objective function mean and variance and it uses parametric tests, such as the ANOVA and the t-test. The same research was made by Czarn et al. (2004) and Ozcelik & Erzurumlu (2006). However, to use parametric statistic tests some conditions must be verified:

- Independence: in statistics, two events are independents when the fact that one occurs does not reduce nor increase the probability of the other one occurring;
- Heteroscedasticity: it indicates that there is no equality of variances between the algorithms;
- Normality: the problem must behave with a Gaussian distribution.

As each algorithm is run without interaction with each other, the independence criterion is guaranteed. The other two can be confirmed by some tests. The heteroscedasticity can be checked using the Levene's test. For the normality it can be chosen one of the following:

- Kolmogorov-Smirnov;
- Shapiro-Wilk;
- D'Agostino-Pearson.

However, those three conditions will hardly be met at the same time. Because of that, García et al. (2007) used non-parametric statistic procedures in the comparison of algorithms results. This author concluded that, even without meeting the normality condition, the results of parametric and non-parametric are similar. García et al. (2007) also suggested that non-parametric analysis be chosen in the case of multi objective functions.

## Chapter 4

# Steel-Concrete Composite I-Girder Bridge Optimization

This chapter describes the steel-concrete composite I-girder optimization problem. The first section shows its variables and formulations. The second section describes the optimization approach developed to solve this problem.

### 4.1 Optimization Problem

The steel-concrete composite I-girder bridge system studied in the present dissertation corresponds to a simply supported straight axis structure. In practical applications, its span usually varies from 20 to 50m (PINHO; BELLEI, 2007). Figure 21 shows a typical cross-section for this structure.

The final cost of the bridge is influenced by more than twenty variables, which can be grouped as follows:

1. Geometric values (see Figures 21, 22, 23 and 24): medium thickness of the deck, considering its haunch ( $h$ ), width between beams ( $b_2$ ), width and thickness of the top flange of the beam ( $b_s$  and  $t_s$ ), height and thickness of the beam web ( $h_v$  and  $t_w$ ), width

and thickness of the bottom flange of the beam ( $b_u$  and  $t_u$ ), the diameter and height of the stud ( $d_{stud}$  and  $h_{stud}$ ), width and thickness of the support stiffener ( $b_{sa}$  and  $t_{sa}$ ), width and thickness of the transversal stiffener ( $b_{st}$  and  $t_{st}$ ), the distance between the support and the first transversal stiffener ( $d_0$ ), the distance between each transversal stiffener ( $d_1$ ), width and thickness of the longitudinal stiffener ( $b_{sl}$  and  $t_{sl}$ ), the profile and the quantity of diaphragms ( $diaf$  and  $n_{diaf}$ );

2. Material characteristics: two variables to define the concrete of the deck and the steel of the beams;
3. Reinforcement: three variables to define the reinforcement of the concrete (longitudinal and transversal positive reinforcement and longitudinal negative reinforcement);
4. The number of the beams used in the bridge.

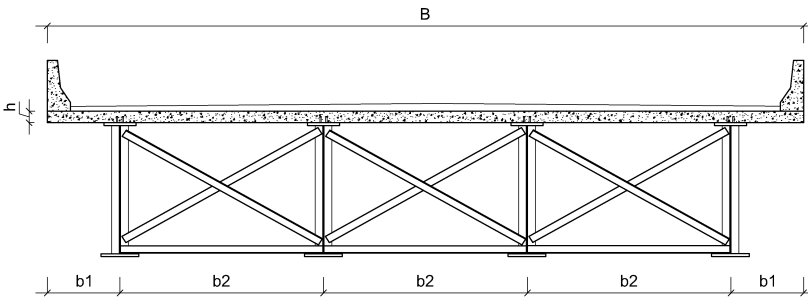


Figure 21 – Bridge cross-section

Some parameters of this study, such as the geometry of the barriers, the thickness of the pavement, the width of the bridge ( $B_{bridge}$ ) and its free span ( $L_b$ ), are fixed quantities and are not subjected to optimization.

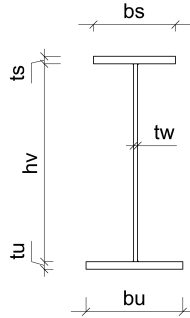


Figure 22 – Beam geometric design variables

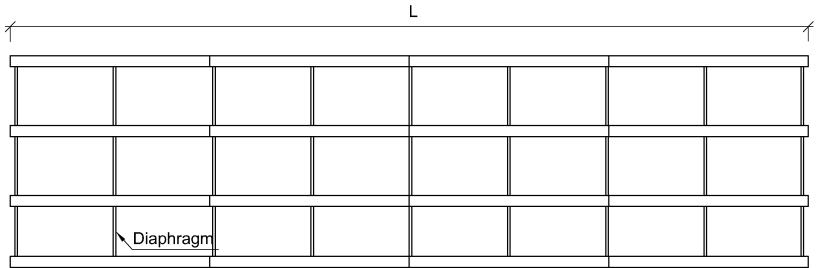


Figure 23 – Bridge top view

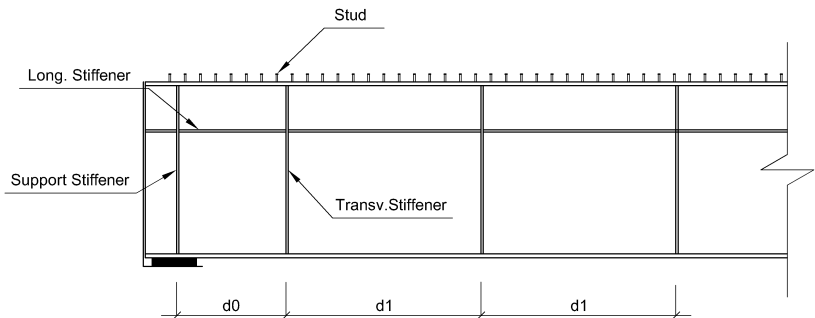


Figure 24 – Beam accessories

The effective width of the slab to integrate the beam composite section furnished by AASHTO is defined by Equation 4.1 and

demonstrated in Figure 25.

$$b_c \leq \begin{cases} \frac{L_b}{4} \\ b_2 \\ 12 \times h \end{cases} \quad (4.1)$$

where  $b_c$  is the composite section slab effective width;  $L_b$  is the span of the bridge;  $b_2$  is the width between girders;  $h$  is the deck thickness

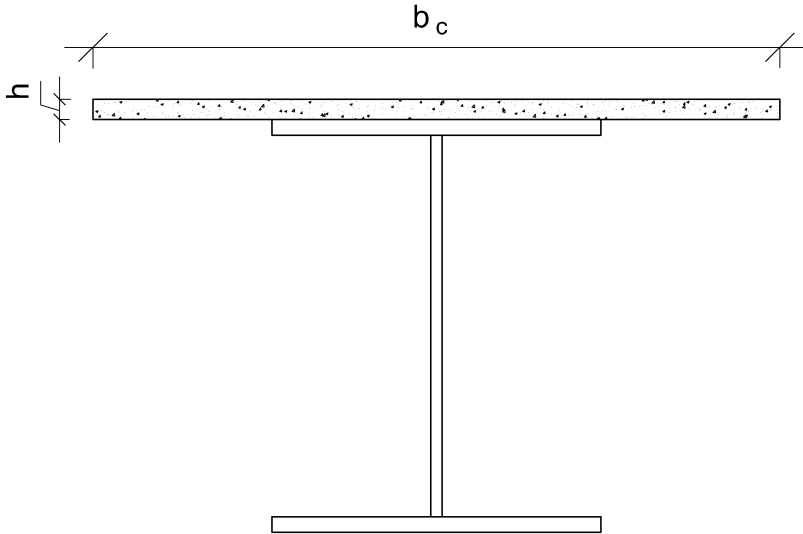


Figure 25 – Composite Section

To find the optimum design of the bridge, the cost of the structure, represented by Equation 4.2, has to be minimized while satisfying the constraints in Equation 4.3.

$$Cost = f(x_1, x_2, \dots, x_n) \quad (4.2)$$

$$g_j(x_1, x_2, \dots, x_n) \leq 0, j = 1, \dots, m \quad (4.3)$$

$$x_d \in \Omega = (dv_1, dv_2, \dots, dv_q) \quad (4.4)$$

$$x_{min} \leq x_k \leq x_{max} \quad (4.5)$$

where  $Cost$  is the cost function;  $g_j$  are the constraints of the problem;  $x_d$  are the discrete variables;  $dv_q$  are the possible discrete values for the variables;  $x_k$  are the continuous variables.

The objective function of this analysis is the cost of the bridge. It is shown in Equation 4.6:

$$Cost = \sum_{i=1}^t p_i \times m_i \quad (4.6)$$

where  $p_i$  are the unit prices;  $m_i$  are the measurements of the units;  $t$  is the total number of construction units.

This function considers the cost of the materials (concrete, steel and reinforcement). These prices are obtained by a survey of costs of civil construction conducted by Caixa Econômica Federal (Federal Economic Fund) and IBGE (Brazilian Institute of Statistics and Geography) every month in Brazil (Caixa Econômica Federal, 2015). The data used is from June 2015 and are given in Table 2. The prices are converted to dollar currency with the exchange price of November 19<sup>th</sup> 2015, which is R\$3.75. Since the cost of the studs are much inferior when compared to the whole structure, its unit cost was simplified taken to be the same as the structural steel employed for the bridge. Despite their importance, the bridge construction costs, for instance, the beams erection costs as well as the form-work cost of the top slab were not included in the Equation 4.6. Then, this assessment would be interesting in further investigations.

The constraints herein applied, which were previously described in Section 2.1.2, are based on AASHTO standards (AASHTO, 2002; AASHTO, 2012).

A penalization scheme is used to transform the constrained optimization problem given by Equation 4.3 into an unconstrained problem. It consists in summing a penalization proportional to the violation to

Table 2 – Prices

Item	Price (R\$)	Price (U\$)
$m^3$ of concrete CA-20	351.20	93.65
$m^3$ of concrete CA-25	364.03	97.07
$m^3$ of concrete CA-30	374.71	99.92
$m^3$ of concrete CA-35	386.46	103.06
kg of steel ASTM A36	4.08	1.09
kg of steel ASTM A572 Gr.50	4.54	1.21
kg of reinforcement steel	6.22	1.66

the objective function. The penalty function is represented by Equation 4.7,

$$P_t(x) = w_{par} \left[ \sum_{i=1}^t \left( 1 - \frac{p_i}{p_i^*} \right)^+ \right] \quad (4.7)$$

where  $w_{par}$  is a positive weight parameter,  $p_i$  is a given structural response,  $p_i^*$  is the standard bound. For this problem it was used a weight factor of  $10^{10}$  to reject those designs that didn't meet the safety conditions.

## 4.2 Two-Stage Based Optimization Approach

To solve an optimization problem, first it is necessary to define a structural evaluation module that can evaluate the stress envelopes and checks all the limit states and geometric constraints. For that, the structure has to be defined by design variables and the constraints have to be evaluated.

It is proposed to couple two different models in the structural evaluation module: a design practice based model and a FEM model. The FEM is able to furnish a more accurate result, but it also demands a much higher computer cost. Then, a single-stage FEM based procedure would be infeasible. In this scheme, the simplified structural model is employed first, aiming to locate an optimum region and provide the



first member to the population created in the next stage. Since this step requires a very low computational time, it is carried out 25 times with a 200,000 objective function evaluations (OFEs) each, without much increase in the time processing. Thus, only the individual that achieved the lowest cost in the first stage is used as a starting point for the next step (FEM model). In this stage, more 1,500 OFEs are performed to find the final optimum solution.

The reader may find below a step-wise algorithm in terms of meta-language:

**Step 1** Initialize the parameters of the meta-heuristic algorithm with the simplified and the FEM model, such as:  $n_{pop,SM}$ ,  $OFE_{SM}^{max}$ ,  $it_{SM}^{max}$ ,  $n_{pop,FEM}$  and  $OFE_{FEM}^{max}$ ;

**Step 2** Call the meta-heuristic with the simplified model using  $\mathbf{X}^k = [\mathbf{x}_1^k, \dots, \mathbf{x}_{n_{pop,SM}}^k]$  as a random initial population and  $OFE_{SM}^{max}$  as stopping criterion;

**Step 3** Save the final population as  $\mathbf{X}^{*k} = [\mathbf{x}_{1,SM}^{*k}, \dots, \mathbf{x}_{n_{pop,SM}}^{*k}]$ , where  $\mathbf{x}_{1,SM}^{*k}$  is the best design found;

**Step 4** Make  $k = k + 1$ ;

**Step 5** If  $k \geq it_{SM}^{max}$ , go to step 6, otherwise return to step 2;

**Step 6** Choose the optimal result from the simplified model best designs  $\mathbf{X}^{*opt} = [\mathbf{x}_{SM}^{*1}, \dots, \mathbf{x}_{SM}^{*it_{SM}^{max}}]$ , where  $\mathbf{x}_{SM}^{*opt}$  is the best design found;

**Step 7** Call the meta-heuristic with the FEM model using as starting point  $\mathbf{x}_{SM}^{*opt}$  and  $OFE_{FEM}^{max}$  as stopping criterion;

**Step 8** Save the best design of the meta-heuristic with FEM model search as  $\mathbf{x}_{FEM}^{*opt}$ ;

**Step 9** Optimal result:  $\mathbf{x}^* = \mathbf{x}_{FEM}^{*opt}$

where  $n_{pop,SM}$  is the size of the population used in the simplified model;  $OFE_{SM}^{max}$  is the maximum objective function evaluations for

each iteration of the simplified model;  $it_{SM}^{max}$  defines how many times the simplified model will run;  $n_{pop,FEM}$  is the size of the population used in the FEM model;  $OF_{FEM}^{max}$  is the maximum objective function evaluations for the FEM model;  $\mathbf{X}^k$  is the population of the  $k^{th}$  iteration of the simplified model and  $[\mathbf{x}_1^k, \dots, \mathbf{x}_{n_{pop,SM}}^k]$  are the members of this population;  $\mathbf{X}^{*k}$  is the final population of the  $k^{th}$  iteration of the simplified model;  $\mathbf{X}^{*opt}$  gathers the best individual of each iteration of the simplified model and  $\mathbf{x}_{SM}^{*opt}$  is the optimum design of the first stage;  $\mathbf{x}_{FEM}^{*opt}$  is the best individual found in the FEM model stage;  $\mathbf{x}^*$  is the optimum design.

The proposed procedure is illustrated in the flowchart of the Figure 26.

Because of the non-convex and multi-modal characteristics of the objective function, the main advantage of the two-stage approach is its ability of combining the benefits furnished by the two different stages. Through this procedure, the optimum design can follow an accurate structural model while using a reasonable computational processing.

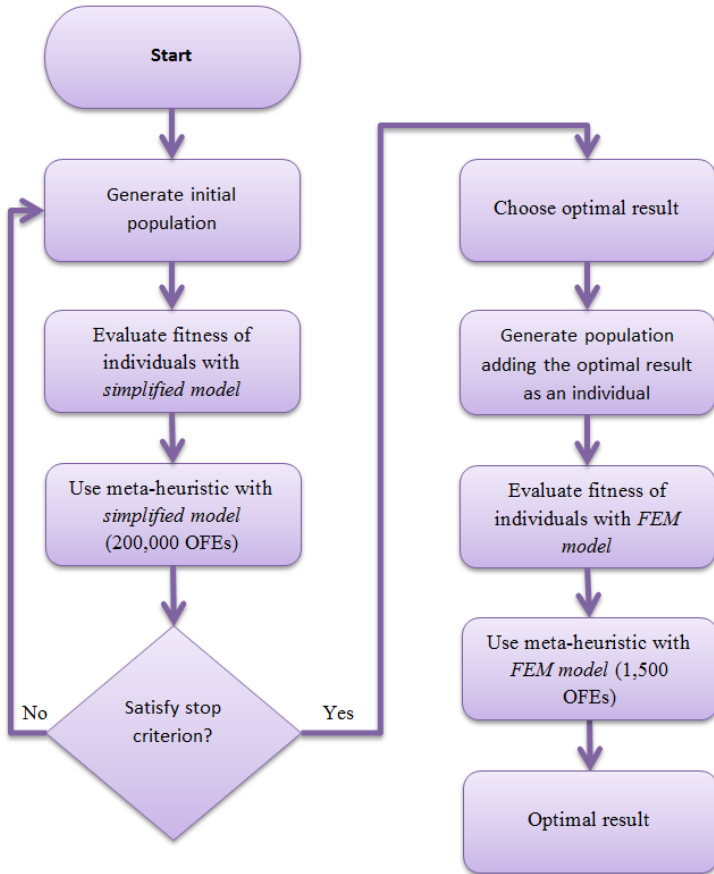


Figure 26 – Optimization procedure flowchart



## Chapter 5

# Numerical Example

This chapter presents the numerical examples used to test the optimization approach developed herein. Firstly, a mechanical model validation is conducted to ascertain the structural model used. Then, the composite bridge is optimized through all the heuristic algorithms described in Section 3.2. The procedure is carried out only using the simplified model to assess the performance of the optimization algorithms for this specific problem. Finally, the composite bridge is designed using the two-stage based optimization approach proposed.

### 5.1 Structure Studied

For illustration purposes, a numerical example of a composite bridge studied in Pinho & Bellei (2007) and Leitão et al. (2011) is evaluated. The structure is 13m wide, has 40m of free span and is composed of 4 plate girders evenly spaced of 3.50m. The deck is 23cm thick, made of concrete CA-25. All the accessories (stud, stiffeners and diaphragm) and the girders are fabricated with the A572 Gr.50 steel. The optimization problem also considered the same load hypotheses as the design of Pinho & Bellei (2007), which are described in Section 2.1.1. Table 9 details all the geometric configuration and Figure 27 shows the cross-section of this bridge.

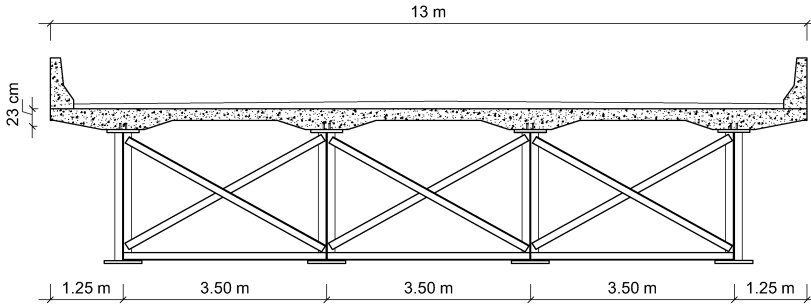


Figure 27 – Cross-section of the bridge studied in Pinho & Bellei (2007) and Leitão et al. (2011)

The bounds imposed on the variables are indicated on Table 3, as well as its increments. Except for the reinforcement variables, all the other ones have discrete values. The bounds of number of beams were imposed because of cantilever deflection limits and minimum beam spacing. The options for the type of concrete and steel are displayed on Table 2; the variable *diaf* represents the choices for equal leg angles, which are [L 101.6x6.35; L 101.6x7.94; L 101.6x9.52; L 101.6x11.11; L 101.6x12.7; L 127x6.35; L 127x7.94; L 127x9.52; L 127x12.7; L 127x15.88; L 127x11.11; L 152.4x9.52; L 152.4x12.7; L 152.4x15.88; L 152.4x19.05]mm; the remain geometric variables ( $t_s$ ,  $t_w$ ,  $t_u$ ,  $t_{sa}$ ,  $t_{st}$  and  $t_{sl}$ ) have its values imposed by the industry: [0.95; 1.27; 1.6; 1.9; 2.22; 2.54; 3.175; 3.81; 5.08; 6.35; 7.62; 10.16]cm.

## 5.2 Mechanical Model Validation

This Section describes conducted tests made to ascertain the accuracy of the structural model constructed to represent the bridge. A careful attention is given to verify the influence of the rigid link introduced to represent the eccentricity between the slab mid-surface and the beam axis.

To assess the accuracy of the FEM model, the original bridge studied by Pinho & Bellei (2007) and Leitão et al. (2011) was identically

Table 3 – Bounds of the variables

Variable	Bounds	Increments
$b_2$	[2, 4]m	0.25 m
Concrete	[CA-20, CA-35]	5 MPa
Steel	[A36, A572 Gr.50]	-
h	[15, 25]cm	1 cm
Long. Positive Reinf.	[0.1, 20] $cm^2$	-
Transv. Positive Reinf.	[0.1, 20] $cm^2$	-
Long. Negative Reinf.	[0.1, 20] $cm^2$	-
# of beams	[4, 6]	1
$b_s$	[30, 100]cm	1 cm
$h_v$	[100, 200]cm	1 cm
$b_u$	[30, 100]cm	1 cm
$d_{stud}$	[1.9, 2.5]cm	0.3 cm
$h_{stud}$	[1, 15]cm	1 cm
$b_{sa}$	[10, 50]cm	1 cm
$b_{st}$	[10, 100]cm	1 cm
$d_0$	[10, 300]cm	1 cm
$d_1$	[10, 300]cm	1 cm
$b_{sl}$	[10, 100]cm	1 cm
$n_{diaf}$	[1, 30]	1

modelled both in the in-house Matlab developed code as well as in SAP2000 analysis software (Figure 28). In the two models:

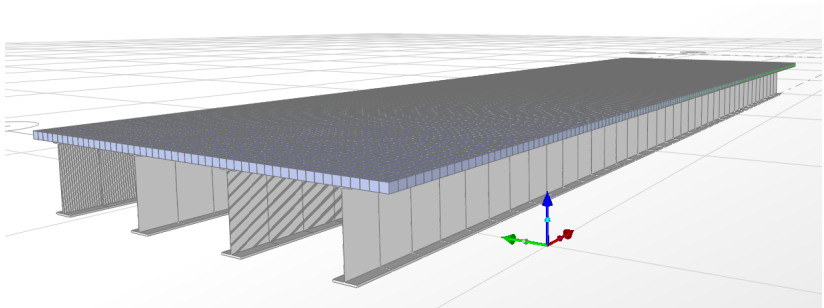


Figure 28 – SAP2000 model

- the bridge deck was represented through 8320, 25x25cm, 4-node, rectangular shell elements;
- each girder was modelled using 640 2-node, 6-DOF, Euler-Bernoulli frame elements (because of its small influence, the shear deformation is not taken into account);
- the eccentricity between the slab mid-surface and the beam axis was considered by introducing a rigid link.

Then, structure is subjected to five random load cases, which are listed below. In each one of them, both models (Matlab and SAP2000) were compared to assess the precision of the response values.

- **Load Case 1:** uniform distributed load of  $10\text{kN/m}^2$  on the entire bridge slab;
- **Load Case 2:** concentrated load of 100kN applied at the mid span of the first girder;
- **Load Case 3:** only the uniform distributed load part of the moving load ( $5\text{kN/m}^2$  on some parts of the slab);
- **Load Case 4:** concentrated load part of the moving load (6 loads of 60kN);
- **Load Case 5:** the moving load.

The results of internal forces and displacements in the second girder are shown in Table 4. Based on that, it is possible to conclude that the in-house Matlab model employed in the present work is accurate and correct (and it is fully in accordance with a very robust computational package SAP2000) to be used in the optimization problem.

Table 5 compares the internal forces found by the FEM model with those furnished by the Level Rule and Fauchart procedures. The difference between bending moments and shear considering the simplified and FEM model were quite large. Note that the design practice



Table 4 – Results

Load	#	SAP2000	Matlab	Difference
Case 1	Bending Moment	4,857.89 kN.m	4,849.60 kN.m	-0.17%
	Shear Force	587.26 kN	584.22 kN	-0.52%
	Displacement	9.39 cm	9.40 cm	0.11%
Case 2	Bending Moment	676.29 kN.m	686.40 kN.m	1.47%
	Shear Force	46.85 kN	46.56 kN	-0.63%
	Displacement	1.07 cm	1.10 cm	2.73%
Case 3	Bending Moment	2,604.83 kN.m	2,624.20 kN.m	0.76%
	Shear Force	299.76 kN	297.92 kN	-0.62%
	Displacement	4.76 cm	4.80 cm	0.83%
Case 4	Bending Moment	2,104.24 kN.m	2,141.80 kN.m	1.75%
	Shear Force	154.09 kN	156.08 kN	-0.65%
	Displacement	4.10 cm	4.22 cm	2.84%
Case 5	Bending Moment	4,709.04 kN.m	4,766.00 kN.m	1.19%
	Shear Force	456.85 kN	454.00 kN	-0.63%
	Displacement	8.86 cm	9.01 cm	1.66%

schemes illustrated are very simple approaches that do not consider major aspects incorporated by FEM analysis as, for instance, the eccentricity between the slab and the girder and the whole consideration of bridge superstructure.

Table 5 – Comparison of internal forces

Item	LR	FM	FEM Matlab	FEM Matlab - without eccentricity
Bending Moment	7,095.80 kN.m	5,927.10 kN.m	4,766.00 kN.m	5,404.00 kN.m
Shear Force	635.55 kN	490.80 kN	454.00 kN	428.07 kN

Finally, the stress distribution provided directly by the FEM model are compared to the results found when using the total bending moment in the girder and the T section geometry furnished by AASHTO (Equation 4.1). Figure 29 shows the stress distribution on the bridge subjected to the moving load in its critical location. Figure 30 shows a zoom with the most critical stresses.

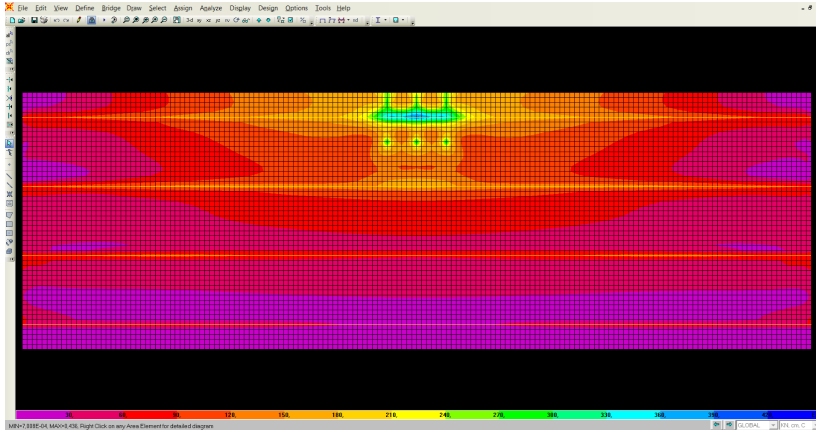


Figure 29 – Stress distribution

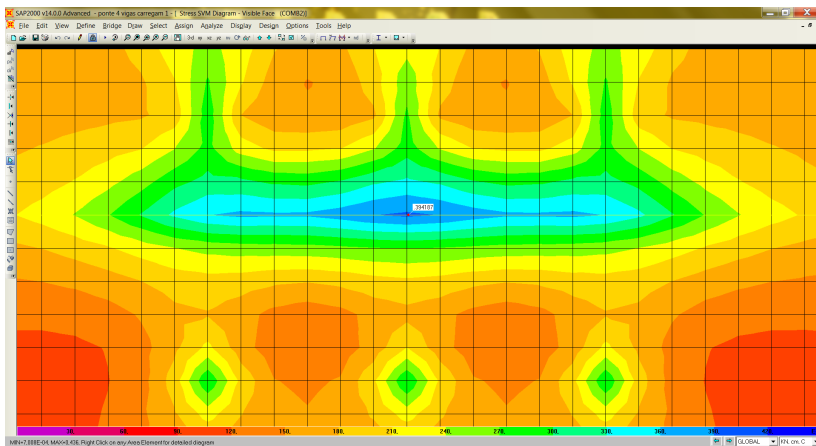


Figure 30 – Stress distribution (zoom)

The FEM model results in a maximum tension stress of  $0.395 \text{ kN/cm}^2$ . For the same case of moving load, using a composite girder with a  $2.50\text{m}$  width concrete slab, the standard cross section reaches  $0.398 \text{ kN/cm}^2$ . Thus, leading to a small difference of only  $0.78\%$ .

### 5.3 Assessment of the Heuristic Algorithms

In order to assess the performance of the meta-heuristic methods explained in Section 3.2 for the specific studied problem, the optimization of the steel-concrete composite I-girder bridge is carried out with all presented algorithms. The used parameters are shown in Table 6. To obtain the statistics, the algorithms are run 25 times with 200,000 objective function evaluations (OFEs). Because of the computer cost of the model all the used results for the statistic tests are obtained applying only the simplified model.

Table 6 – Algorithms Parameters

<b>BSA</b>	<b>FA</b>	<b>GA</b>	<b>ICA</b>	<b>SGA</b>
Pop.=100	Pop.=100	Pop.=100	Pop.=100	Pop.=100
Dim_Rate=1	Alpha=0.5	Crossover=100	Imperialists=10	Alpha_Min.=0.01
	Beta=0.2	Mutation=20	Rev_Rate=0.3	Alpha_Init.=3
	Gamma=1		Assim_Coef.=2	Global_It_Ratio=0.4
			Angle_Coef.=0.5	SG_Ratio=0.1
			Zeta=0.01	N_Perturbed=5
			Damp_Ratio=0.99	
			Uniting=0.02	
			Zarib=1.05	
			Alpha=0.1	

Using the prices shown in Table 2 the cost of the original structure, shown in Section 5.1, is estimated in R\$482,626.33 or U\$128,700.35. The results found by the optimization algorithms are shown in Table 7, and the convergence curves of all the algorithms are demonstrated in Figure 31.

Table 7 – Results for 200,000 OFEs

<b>Item</b>	<b>BSA (U\$)</b>	<b>FA (U\$)</b>	<b>GA (U\$)</b>	<b>ICA (U\$)</b>	<b>SGA (U\$)</b>
Maximum	158,760.13	173,760.04	184,821.16	231,039.28	160,469.65
Median	143,424.43	143,412.66	161,169.16	182,542.25	146,683.26
Minimum	133,067.57	131,309.99	138,078.27	154,312.95	126,750.23
SD	5,310.32	13,103.92	11,978.20	19,442.53	11,529.06

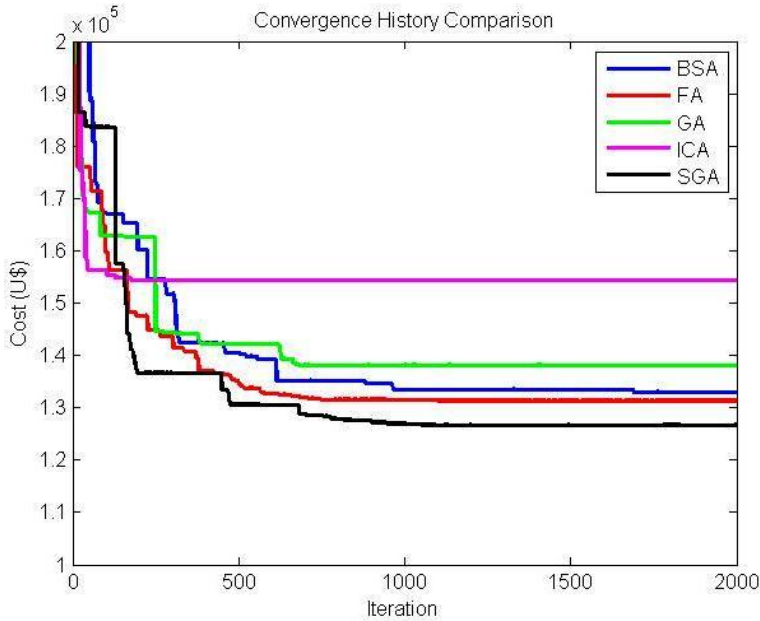


Figure 31 – Convergence history comparison of all the algorithms used

The normality tests Kolmogorov-Smirnov, Shapiro-Wilk and D'Agostino-Pearson are conducted in all of the groups of data, using the null hypothesis "the data are not under a Gaussian distribution". The first test couldn't reject the null hypothesis, but the Shapiro-Wilk and D'Agostino-Pearson tests concluded that the data have a normal distribution with a p-value minor than 0.05. Because of that, for the comparison of the algorithms the parametric ANOVA test is conducted with the null hypothesis "there is no significant difference between the algorithms".

Figure 32 has a box representing the results of the ANOVA analysis for each algorithm. The central mark of the box is the median, the edges are the 25<sup>th</sup> and 75<sup>th</sup> percentiles, the whiskers extend to the most extreme data points not considering outliers, and the outliers are plotted individually. Table 8 indicates that the p-value (Prob>F) is

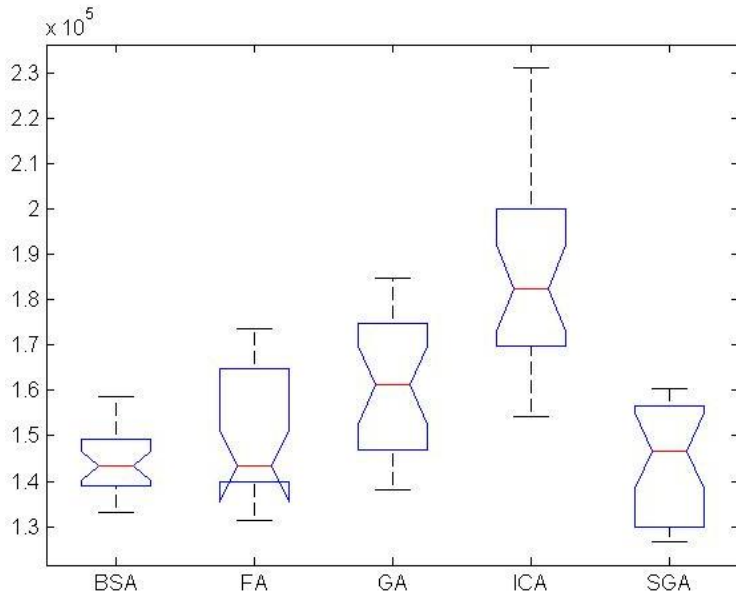


Figure 32 – Results of the ANOVA test for 200,000 OFEs

Table 8 – Results of the ANOVA test for 200,000 OFEs

Source	SS	df	MS	F	Prob>F
Columns	3.30923E+10	4	8.27308E+09	35.19	1.99468E-19
Error	2.82114E+10	120	2.35095E+08		
Total	6.13038E+10	124			

very small, which means that the results of the algorithms cannot be considered equivalents. Figure 33 shows that the means between the BSA, the FA and the SGA are not significantly different. That means that these three were the best performed algorithms for this problem. Comparing them, the SGA is able to find the best result. On the other hand, the BSA has the lowest standard deviation and its maximum result is the lowest of them all. Hence, both BSA and SGA can be considered good choices as an optimization tool for this specific problem.

In this dissertation the SGA is chosen to be used in the next stages.

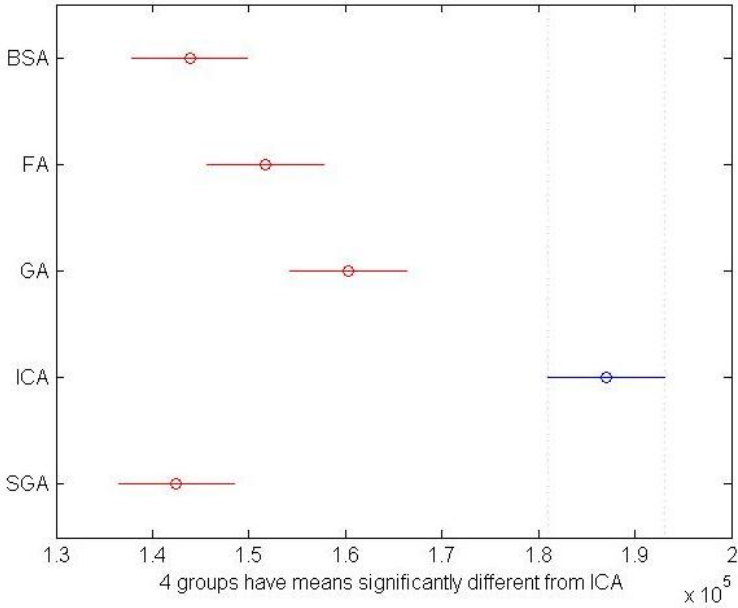


Figure 33 – Comparison of the means of the algorithms

## 5.4 Two-stage Bridge Optimization

The proposed two-stage optimization procedure is employed to the studied bridge. The preliminary results are obtained with the simplified model and the final optimized design is calculated with the FEM model. The first stage (simplified model) is composed of 26 variables, as described in Section 4.1, and with the bounds indicated in Section 5.1. The second stage uses a FEM mesh composed by 4,160 shell elements with the dimensions 25 x 50cm; it has the same bounds as the previous one, but now only considering 24 design variables. The number of beams and width between beams ( $b_2$ ) are fixed as equal the best solution found on the first stage. This FEM mesh was chosen to provide accuracy with a reasonable computational cost.

Because the original design was developed using the Allowable Stress Design (ASD) approach, the ensuing analysis is divided in two sections. First, to properly compare the optimum results to the original bridge, the ASD constraints are employed. Then, the bridge is also optimized through the Limit and Resistance Factor Design (LRFD) method, to demonstrate the influence of a most modern design philosophy on the final result.

#### 5.4.1 Allowable Stresses

##### a) Level Rule in first stage

The Level Rule is adopted to optimize the first stage as a first attempt. This maintains the same conditions of the original design, which allows a fair comparison of results. Table 9 shows the original design solutions as well as the best result of both stages (LR + FEM) using the SGA. Figure 34 demonstrates the convergence history of both optimization stages. A more detailed comparison of costs is shown in Table 10.

The optimum design led to use of a thinner slab ( $h$ ) with a stronger concrete. It also resulted in a thicker beam web ( $t_w$ ). Thus, longitudinal stiffeners are not required.

The second stage, FEM model considering eccentricity, is able to reduce more 3% than the original design, because there is reduction in the girder stresses up to 30% (Table 11). This is slightly worse than the previous 3 girders configuration.

##### b) Fauchart approach in first stage

The original bridge internal forces calculated in Section 5.2, showed that the Fauchart Model leads to lower results than those observed from the Level Rule. Then, as a second attempt, the bridge will be optimized through this simplified procedure in the first stage. The results are presented in Table 12.

In this scenario, the first stage chose the 4 girders configuration, as the solution proposed by the manual design. Furthermore, it employed a thinner slab with a more resistant concrete, as the previous optimizations.

Table 9 – Comparison of design solutions with 4 beams - Allowable Stresses

Item	Pinho & Bellei (2007)	LR (SGA)	FEM (SGA)
$b_1$	1.25m	1.25m	1.25m
$b_2$	3.50m	3.50m	3.50m
Concrete	CA-25	CA-35	CA-35
Steel	A572 Gr.50	A572 Gr.50	A572 Gr.50
h	23cm	18cm	20cm
Long. Positive Reinf.	$8.00cm^2$	$9.75cm^2$	$8.51cm^2$
Transv. Positive Reinf.	$5.00cm^2$	$4.51cm^2$	$4.02cm^2$
Long. Negative Reinf.	$13.00cm^2$	$17.27cm^2$	$15.41cm^2$
# of beams	4	4	4
$b_s$	50cm	41cm	48cm
$t_s$	2.54cm	2.22cm	2.22cm
$h_v$	193cm	200cm	199cm
$t_w$	0.95cm	1.60cm	1.60cm
$b_u$	67cm	47cm	47cm
$t_u$	5.08cm	6.35cm	5.08cm
Stud	2.2x15cm	2.2x10cm	2.2x10cm
Support stiffener	20x2.22cm	11x2.22cm	14x2.22cm
Transversal stiffener	17x1.27cm	12x1.27cm	13x0.95cm
Longitudinal stiffener	17x1.27cm	None	None
Diaphragm	127x127x9.52cm	127x127x6.35cm	127x127x7.94cm
Cost	U\$128,700.35	U\$128,553.19	U\$124,285.64
% Comparison	-	-0.11%	-3.55%

Table 10 – Comparison of costs

Item	Pinho & Bellei (2007)	LR (SGA)	FEM (SGA)
Concrete	U\$11,610.13	U\$9,646.13	U\$10,717.87
Reinforcing Steel	U\$615.87	U\$692.05	U\$614.29
Frame Steel	U\$95,241.92	U\$107,882.67	U\$100,925.33
Accessories	U\$21,232.43	U\$10,332.33	U\$12,027.30
Total Cost	U\$128,700.35	U\$128,553.19	U\$124,285.64

Table 11 – Comparison of internal forces

Item	LR Model	FEM Matlab
Moment	7,096 kN.m	4,938 kN.m
Shear	724 kN	599 kN



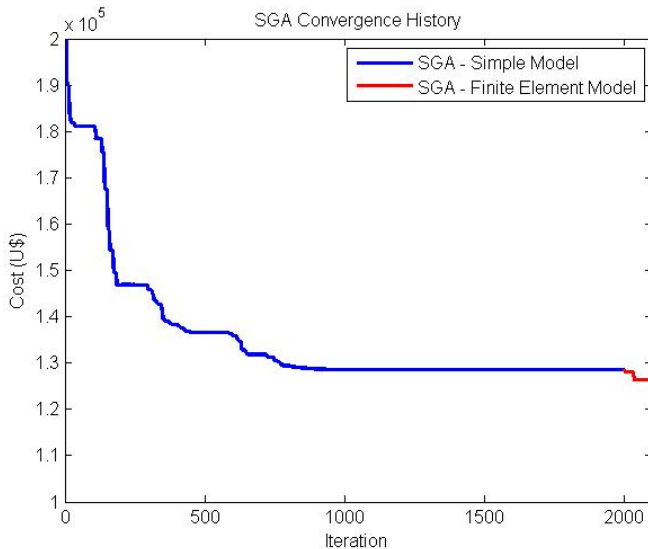


Figure 34 – Convergence history of the two-stage based optimization

Another common feature is the use of a thicker beam web. Though, the longitudinal stiffeners are employed.

As previously observed, the Fauchart Model is closer to the FEM model than the Level Rule. This makes the optimization tool reach better results already in the first stage (7.43%). Nonetheless, a slight difference in the girder stresses still remains. Table 13 shows a variation up to 17% in the bending moment. Thus, the use of the more refined model can still guarantee a cheaper solution (9.17%).

#### 5.4.2 Limit and Resistance Factor Design

The original bridge was designed using the classical ASD methodology. Thus, to assess the influence of a more recent code edition on the bridge optimum solution, the AASHTO (2012) LRFD constraints are also considered, in accordance with Toma, Duan & Chen (1999). Initially, the original bridge is verified using the AASHTO LRFD recommendations. It is found that this structure does not meet the support

Table 12 – Comparison of design solutions using Fauchart - Allowable Stresses

Item	Pinho & Bellei (2007)	FM (SGA)	FEM (SGA)
$b_1$	1.25m	1.25m	1.25m
$b_2$	3.50m	3.50m	3.50m
Concrete	CA-25	CA-35	CA-35
Steel	A572 Gr.50	A572 Gr.50	A572 Gr.50
h	23cm	18cm	20cm
Long. Positive Reinf.	8.00cm <sup>2</sup>	9.70cm <sup>2</sup>	9.21cm <sup>2</sup>
Transv. Positive Reinf.	5.00cm <sup>2</sup>	4.50cm <sup>2</sup>	4.02cm <sup>2</sup>
Long. Negative Reinf.	13.00cm <sup>2</sup>	17.30cm <sup>2</sup>	17.05cm <sup>2</sup>
# of beams	4	4	4
$b_s$	50cm	44cm	42cm
$t_s$	2.54cm	2.22cm	2.22cm
$h_v$	193cm	198cm	196cm
$t_w$	0.95cm	1.27cm	1.27cm
$b_u$	67cm	37cm	34cm
$t_u$	5.08cm	7.62cm	7.62cm
Stud	2.2x15cm	2.2x13cm	2.2x13cm
Support stiffener	20x2.22cm	11x2.54cm	13x2.22cm
Transversal stiffener	17x1.27cm	12x0.95cm	12x0.95cm
Longitudinal stiffener	17x1.27cm	15x1.27cm	15x1.27cm
Diaphragm	127x127x9.52cm	127x127x6.35cm	127x127x6.35cm
Cost	U\$128,700.35	U\$119,796.43	U\$117,884.93
% Comparison	-	-7.43%	-9.17%

Table 13 – Comparison of internal forces

Item	Fauchart Model	FEM Matlab
Moment	5,910 kN.m	4,864 kN.m
Shear	603 kN	598 kN

and transversal stiffeners, the beam web slenderness and the beam ductility requirements.

Then, the optimization procedure is carried out using both simplified models in first stage for comparison. The results are presented in Table 14 and 15 for Level Rule and Fauchart, respectively.

In the first test, the final cost was U\$ 154,535.35 using a 4 girders configuration. Once again, it used a thick beam web without longitudinal stiffeners. The biggest difference between the LRFD design and the ASD is the thickness of the top and bottom flanges. The former resulted in

Table 14 – LRFD design using Level Rule Model on first stage

Item	LR (SGA)	FEM (SGA)
$b_1$	1.25m	1.25m
$b_2$	3.50m	3.50m
Concrete	CA-35	CA-35
Steel	A36	A36
h	17cm	16cm
Long. Positive Reinf.	10.51 $cm^2$	11.42 $cm^2$
Transv. Positive Reinf.	4.92 $cm^2$	5.58 $cm^2$
Long. Negative Reinf.	18.57 $cm^2$	20.15 $cm^2$
# of beams	4	4
$b_s$	51cm	47cm
$t_s$	10.16cm	10.16cm
$h_v$	200cm	189cm
$t_w$	1.90cm	1.90cm
$b_u$	92cm	93cm
$t_u$	2.22cm	1.90cm
Stud	1.9x9cm	1.9x10cm
Support stiffener	15x2.54cm	18x2.54cm
Transversal stiffener	19x6.35cm	21x6.35cm
Longitudinal stiffener	None	None
Diaphragm	127x127x6.35cm	127x127x7.94cm
Cost	U\$167,619.59	U\$154,535.35
% Comparison	-	-8.47%

10.16cm for the top flange and 1.90cm for the bottom one. This thickness in the top flange is determined mostly due to the AASHTO ductility constraint, which aims to prevent permanent crashing of the concrete slab when the composite section approaches its plastic moment capacity. Because this restriction is not adopted in the Brazilian Standard NBR 8800 (ABNT, 2008), then, in that applications, the top flange dimensions become usually lower when compared to the bottom one.

As observed when applying ASD constraints, the FEM model employed in the second stage, lead to an important bridge saving costs. In this scenario, the difference of 8.47% is achieved. Table 16 shows a

Table 15 – LRFD design using Fauchart Model on first stage

Item	FM (SGA)	FEM (SGA)
$b_1$	1.25m	1.25m
$b_2$	3.50m	3.50m
Concrete	CA-35	CA-35
Steel	A36	A36
h	18cm	17cm
Long. Positive Reinf.	$10.63cm^2$	$10.82cm^2$
Transv. Positive Reinf.	$4.86cm^2$	$4.94cm^2$
Long. Negative Reinf.	$18.79cm^2$	$20.12cm^2$
# of beams	4	4
$b_s$	72cm	61cm
$t_s$	6.35cm	7.62cm
$h_v$	200cm	193cm
$t_w$	1.90cm	1.90cm
$b_u$	73cm	78cm
$t_u$	2.22cm	2.22cm
Stud	2.2x9cm	2.2x14cm
Support stiffener	34x2.54cm	42x3.175cm
Transversal stiffener	33x3.81cm	25x3.175cm
Longitudinal stiffener	None	None
Diaphragm	127x127x6.35cm	127x127x6.35cm
Cost	U\$154,444.34	U\$153,653.33
% Comparison	-	-0.46%

18% variation in the bending moments.

Table 16 – Comparison of internal forces

Item	LR Model	FEM Matlab
Moment	7,096 kN.m	5,755 kN.m
Shear	724 kN	599 kN

The LRFD design with the Fauchart also resulted in a 4 girder configuration with a thicker top flange. However, it was able to reach a better overall result. The U\$153,653.33 cost is 0.6% cheaper than the

results using the first model (LR). On the other hand, in this scenario, both the Fauchart and FEM models are quite similar. Table 17 shows little variation in internal forces.

Table 17 – Comparison of internal forces

<b>Item</b>	<b>Fauchart Model</b>	<b>FEM Matlab</b>
Moment	5,691 kN.m	5,732 kN.m
Shear	581 kN	565 kN

Due to these differences, the AASHTO LRFD resulted in a more expensive result than that previously best solution. Even so, the proposed two-stage optimization approach could improve the result found when employing only the simplified approach.



## Chapter 6

# Concluding Remarks and Future Developments

### 6.1 Concluding Remarks

This dissertation presented an efficient two-stage optimization based approach to design steel-concrete composite I-girder bridges. In the first step, a simplified structural model usually adopted by bridge designers was employed aiming to locate an optimum region and to provide a starting point to the next stage. Then, a finite element model (FEM) was used to refine and improve the optimization. The main advantage of this procedure was that it allows combining the low computational cost required on first stage with the accuracy provided on second stage.

Despite it was conceived to steel-concrete composite I-girder bridges, the main idea of combining a simplified structural analysis procedure with a FEM model, in a context of an optimization procedure, is general and it can be adapted to other kinds of structural engineering problems. One of the crucial parts in this scheme is finding an adequate balance (accuracy versus computational time required) between the structural analysis modules chosen for both stages. This will be determinant on the success of the optimization final result. Indeed, this will depend on

the particular problem and must be carefully assessed and examined by the researcher. Note that this is an incipient idea and further studies must be encouraged, due to the promising achieved results.

Due to its non-convex nature and to the presence of discrete variables, the problem required the utilization of a global optimization algorithm. Then, the performance of five well-known meta-heuristic algorithms for this specific problem was evaluated: Backtracking Search Algorithm (BSA), Firefly Algorithm (FA), Genetic Algorithm (GA), Imperialist Competitive Algorithm (ICA) and Search Group Algorithm (SGA). Then, another contribution was the assessment of five modern optimization algorithms for a real world structural problem. The use of statistic tests provided additional information, supporting to correctly choose the best algorithm for the study (BSA and SGA).

For illustration purposes, a numerical example of a composite bridge studied in Pinho & Bellei (2007) and Leitão et al. (2011) was assessed. It was verified that when using a more accurate simplified model in the first stage, with a closer behavior of FEM model, better results can be achieved. In addition, the optimum values had been improved with FEM because it provided lower internal forces to the girders (a bending moment reduction around 30%). When using the Level Rule in the first stage, the proposed scheme was able to reduce 0.11% of the structural cost, reaching up to 3.55% of saving costs in the end of the optimization procedure, when compared to the solution designed manually by a senior engineer. On the other hand, in the scenario using the Fauchart approach, which is closer to the FEM model, the optimization was able to reduce to 7.43% of the structural cost in the first stage, reaching up to 9.17%. Furthermore, the optimal solution reached here is feasible to a direct industrial application. Then, the obtained results showed that the proposed method is very promising and further efforts must be carried out.

Finally, it is important to emphasize that the proposed scheme has shown a valuable tool to assist the engineer (not to substitute) in his day-to-day practice. For instance, the designer can define the variables



of his preferences and use the optimization procedure as a starting point to his own design.

## 6.2 Future Studies

Despite the promising results found in this dissertation, more studies should be made to improve the work. Among them:

- The consideration of dynamic loads;
- Other types of bridges should be added to the optimization process;
- Girders with different sizes should be used to optimize even more the structure;
- Consideration of fabrication costs.



# References

- AASHTO. *Standard specifications for highway bridges*. [S.l.]: American Association of State Highway and Transportation Officials, 2002.
- AASHTO. *Standard specifications for highway bridges*. [S.l.]: American Association of State Highway and Transportation Officials, 2012.
- ABNT. NBR 7188 – carga móvel em ponte rodoviária e passarela de pedestre. *Associação Brasileira de Normas Técnicas, Rio de Janeiro, Brazil. (In portuguese)*, 1984.
- ABNT. NBR 7187 – reinforced and pre-stressed concrete bridge design. *Associação Brasileira de Normas Técnicas, Rio de Janeiro, Brazil. (In portuguese)*, 2003.
- ABNT. NBR 8800 – projeto de estruturas de aço e de estruturas mistas de aço e concreto de edifícios. *Associação Brasileira de Normas Técnicas, Rio de Janeiro, Brazil. (In portuguese)*, 2008.
- ARORA, J. *Introduction to optimum design*. [S.l.]: Academic Press, 2004.
- ATASHPAZ-GARGARI, E.; LUCAS, C. Imperialist competitive algorithm: an algorithm for optimization inspired by imperialistic competition. In: IEEE. *Evolutionary computation, 2007. CEC 2007. IEEE Congress on*. [S.l.], 2007. p. 4661–4667.
- BALDOMIR, A.; HERNANDEZ, S.; NIETO, F.; JURADO, J. Cable optimization of a long span cable stayed bridge in la coruña (spain). *Advances in Engineering Software*, Elsevier, v. 41, n. 7, p. 931–938, 2010.
- BALLING, R. J.; BRIGGS, R. R.; GILLMAN, K. Multiple optimum size/shape/topology designs for skeletal structures using a genetic algorithm. *Journal of Structural Engineering*, American Society of Civil Engineers, v. 132, n. 7, p. 1158–1165, 2006.
- BARTHOLOMEW, P.; MORRIS, A. A unified approach to fully-stressed design. *Engineering Optimization*, Taylor & Francis, v. 2, n. 1, p. 3–15, 1976.

- BHATTI, M. A. A mathematica based environment for analysis and optimum design of composite structures. *Computer Aided Optimum Design of Structures VI*, Computational Mechanics, p. 301, 1999.
- CAI, H.; AREF, A. J. On the design and optimization of hybrid carbon fiber reinforced polymer-steel cable system for cable-stayed bridges. *Composites Part B: Engineering*, Elsevier, v. 68, p. 146–152, 2015.
- Caixa Econômica Federal. Sinapi: índices da construção civil. *Rio de Janeiro: CAIXA*, 2015.
- CHEN, W.-F.; DUAN, L.; ALTMAN, S. *Bridge Engineering Handbook*. [S.l.]: CRC Press, 2000.
- CHENG, B.; QIAN, Q.; SUN, H. Steel truss bridges with welded box-section members and bowknot integral joints, part ii: Minimum weight optimization. *Journal of Constructional Steel Research*, Elsevier, v. 80, p. 475–482, 2013.
- CHENG, J. Optimum design of steel truss arch bridges using a hybrid genetic algorithm. *Journal of Constructional Steel Research*, Elsevier, v. 66, n. 8, p. 1011–1017, 2010.
- CIVICIOGLU, P. Backtracking search optimization algorithm for numerical optimization problems. *Applied Mathematics and Computation*, Elsevier, v. 219, n. 15, p. 8121–8144, 2013.
- COOK, R. D.; MALKUS, D. S.; PLESHA, M. E.; WITT, R. J. *Concepts and applications of finite element analysis*. [S.l.]: John Wiley & Sons, 2007.
- CZARN, A.; MACNISH, C.; VIJAYAN, K.; TURLACH, B.; GUPTA, R. Statistical exploratory analysis of genetic algorithms. *Evolutionary Computation, IEEE Transactions on*, IEEE, v. 8, n. 4, p. 405–421, 2004.
- ELLOBODY, E. *Finite Element Analysis and Design of Steel and Steel-Concrete Composite Bridges*. [S.l.]: Butterworth-Heinemann, 2014.
- FABEANE, R. *Pontes mistas de aço-concreto: estudo de diretrizes para dimensionamento otimizado*. Dissertation — Universidade de Passo Fundo, 2015.
- FERNANDES, W. L. Software para análise e dimensionamento de vigas mistas aço-concreto em pontes rodoviárias. Programa de Pós

Graduação em Engenharia Civil. Departamento de Engenharia Civil, Escola de Minas, Universidade Federal de Ouro Preto., 2008.

FERREIRA, A. J. *MATLAB codes for finite element analysis: solids and structures*. [S.l.]: Springer Science & Business Media, 2008. v. 157.

FURUKAWA, K.; SUGIMOTO, H.; INOUE, K.; YAMADA, Y. Optimization of cable prestresses of cable stayed bridges based on minimum strain energy criterion. In: ASCE. *Computer Utilization in Structural Engineering*. [S.l.], 1989. p. 227–236.

GARCÍA, S.; MOLINA, D.; LOZANO, M.; HERRERA, F. An experimental study on the use of non-parametric tests for analyzing the behaviour of evolutionary algorithms in optimization problems. In: *Proceedings of the Spanish Congress on Metaheuristics, Evolutionary and Bioinspired Algorithms (MAEB'2007)*. [S.l.: s.n.], 2007. p. 275–285.

GOCÁL, J.; ĎURŠOVÁ, A. Optimisation of transversal disposition of steel and concrete composite road bridges. *Procedia Engineering*, Elsevier, v. 40, p. 125–130, 2012.

GONÇALVES, M. S.; LOPEZ, R. H.; MIGUEL, L. F. F. Search group algorithm: a new metaheuristic method for the optimization of truss structures. *Computers & Structures*, Elsevier, v. 153, p. 165–184, 2015.

GUO, H.; LI, Z. Structural topology optimization of high-voltage transmission tower with discrete variables. *Structural and Multidisciplinary Optimization*, Springer, v. 43, n. 6, p. 851–861, 2011.

HAFTKA, R. T. Integrated nonlinear structural analysis and design. *AIAA journal*, v. 27, n. 11, p. 1622–1627, 1989.

HASSAN, M. Optimization of stay cables in cable-stayed bridges using finite element, genetic algorithm, and b-spline combined technique. *Engineering Structures*, Elsevier, v. 49, p. 643–654, 2013.

HOLLAND, J. H. *Adaptation in natural and artificial systems*. [S.l.]: University of Michigan Press, 1975.

HUANG, M.; LI, Q.; CHAN, C.; LOU, W.; KWOK, K.; LI, G. Performance-based design optimization of tall concrete framed structures subject to wind excitations. *Journal of Wind Engineering and Industrial Aerodynamics*, Elsevier, v. 139, p. 70–81, 2015.

- KAVEH, A.; ABADI, A. S. M. Cost optimization of a composite floor system using an improved harmony search algorithm. *Journal of Constructional Steel Research*, Elsevier, v. 66, n. 5, p. 664–669, 2010.
- KAVEH, A.; BEHNAM, A. Design optimization of reinforced concrete 3d structures considering frequency constraints via a charged system search. *Scientia Iranica*, Elsevier, v. 20, n. 3, p. 387–396, 2013.
- KAVEH, A.; MANIAT, M.; NAEINI, M. A. Cost optimum design of post-tensioned concrete bridges using a modified colliding bodies optimization algorithm. *Advances in Engineering Software*, Elsevier, v. 98, p. 12–22, 2016.
- KELESOGLU, O. Fuzzy multiobjective optimization of truss-structures using genetic algorithm. *Advances in Engineering Software*, Elsevier, v. 38, n. 10, p. 717–721, 2007.
- KLINSKY, G. E. R. G. *Uma contribuição ao estudo das pontes em vigas mistas*. Tese (Doutorado) — Universidade de São Paulo, 1999.
- KOCIECKI, M.; ADELI, H. Two-phase genetic algorithm for size optimization of free-form steel space-frame roof structures. *Journal of Constructional Steel Research*, Elsevier, v. 90, p. 283–296, 2013.
- KODIYALAM, S.; VANDERPLAATS, G. N. Shape optimization of three-dimensional continuum structures via force approximation techniques. *AIAA journal*, v. 27, n. 9, p. 1256–1263, 1989.
- KRAVANJA, S.; TURKALJ, G.; ŠILIH, S.; ŽULA, T. Optimal design of single-story steel building structures based on parametric minlp optimization. *Journal of constructional steel research*, Elsevier, v. 81, p. 86–103, 2013.
- KRIPKA, M.; MEDEIROS, G. F.; LEMONGE, A. C. Use of optimization for automatic grouping of beam cross-section dimensions in reinforced concrete building structures. *Engineering Structures*, Elsevier, v. 99, p. 311–318, 2015.
- KUSANO, I.; BALDOMIR, A.; JURADO, J. A.; HERNÁNDEZ, S. Reliability based design optimization of long-span bridges considering flutter. *Journal of Wind Engineering and Industrial Aerodynamics*, Elsevier, v. 135, p. 149–162, 2014.
- LEE, K. S.; GEEM, Z. W. A new meta-heuristic algorithm for continuous engineering optimization: harmony search theory and

- practice. *Computer methods in applied mechanics and engineering*, Elsevier, v. 194, n. 36, p. 3902–3933, 2005.
- LEITÃO, F.; SILVA, J. D.; VELLASCO, P. d. S.; ANDRADE, S. D.; LIMA, L. D. Composite (steel–concrete) highway bridge fatigue assessment. *Journal of Constructional Steel Research*, Elsevier, v. 67, n. 1, p. 14–24, 2011.
- LIU, K.; REYNDERS, E.; ROECK, G. D.; LOMBAERT, G. Experimental and numerical analysis of a composite bridge for high-speed trains. *Journal of sound and vibration*, Elsevier, v. 320, n. 1, p. 201–220, 2009.
- LIU, X.; FAN, J.; NIE, J.; LI, G. Behavior of composite rigid frame bridge under bi-directional seismic excitations. *Journal of Traffic and Transportation Engineering (English Edition)*, Elsevier, v. 1, n. 1, p. 62–71, 2014.
- LOPEZ, R.; LUERSEN, M.; CURSI, E. Optimization of laminated composites considering different failure criteria. *Composites Part B: Engineering*, Elsevier, v. 40, n. 8, p. 731–740, 2009.
- LUTE, V.; UPADHYAY, A.; SINGH, K. K. Computationally efficient analysis of cable-stayed bridge for ga-based optimization. *Engineering Applications of Artificial Intelligence*, Elsevier, v. 22, n. 4, p. 750–758, 2009.
- MADRAZO-AGUIRRE, F.; RUIZ-TERAN, A. M.; WADEE, M. A. Dynamic behaviour of steel–concrete composite under-deck cable-stayed bridges under the action of moving loads. *Engineering Structures*, Elsevier, v. 103, p. 260–274, 2015.
- MARTÍ, J. V.; GONZALEZ-VIDOSA, F.; YEPES, V.; ALCALÁ, J. Design of prestressed concrete precast road bridges with hybrid simulated annealing. *Engineering Structures*, Elsevier, v. 48, p. 342–352, 2013.
- MARTÍNEZ, F. J.; GONZÁLEZ-VIDOSA, F.; HOSPITALER, A.; ALCALÁ, J. Design of tall bridge piers by ant colony optimization. *Engineering Structures*, Elsevier, v. 33, n. 8, p. 2320–2329, 2011.
- MARTINS, A.; SIMÕES, L.; NEGRÃO, J. Optimization of cable forces on concrete cable-stayed bridges including geometrical nonlinearities. *Computers & Structures*, Elsevier, v. 155, p. 18–27, 2015.

- MIGUEL, L. F. F.; LOPEZ, R. H.; MIGUEL, L. F. F. Multimodal size, shape, and topology optimisation of truss structures using the firefly algorithm. *Advances in Engineering Software*, Elsevier, v. 56, p. 23–37, 2013.
- MOURA, M. W.; FERREIRA, M. W.; REAL, M. d. V.; SANTOS, G. C. Comparação do método de fauchart e do método dos elementos finitos na avaliação da distribuição de esforços transversais em pontes rodoviárias. *IX Congresso Brasileiro de Pontes e Estruturas, Rio de Janeiro, Brasil*, 2016.
- MUNCK, M. D.; SUTTER, S. D.; VERBRUGGEN, S.; TYSMANS, T.; COELHO, R. F. Multi-objective weight and cost optimization of hybrid composite-concrete beams. *Composite Structures*, Elsevier, v. 134, p. 369–377, 2015.
- OEHLERS, D. J. Deterioration in strength of stud connectors in composite bridge beams. *Journal of structural engineering*, American Society of Civil Engineers, v. 116, n. 12, p. 3417–3431, 1990.
- OZCELIK, B.; ERZURUMLU, T. Comparison of the warpage optimization in the plastic injection molding using anova, neural network model and genetic algorithm. *Journal of materials processing technology*, Elsevier, v. 171, n. 3, p. 437–445, 2006.
- PEDRO, R. L.; DEMARCHE, J.; MIGUEL, L. F. F.; LOPEZ, R. H. An efficient approach for the optimization of simply supported steel-concrete composite i-girder bridges. *Advances in Engineering Software*, Elsevier, X, n. X, p. X–X, 2017.
- PINHO, F. O.; BELLEI, I. H. *Pontes e viadutos em vigas mistas*. [S.l.]: Instituto Brasileiro de Siderurgia, 2007.
- POITRAS, G.; LEFRANÇOIS, G.; CORMIER, G. Optimization of steel floor systems using particle swarm optimization. *Journal of Constructional Steel Research*, Elsevier, v. 67, n. 8, p. 1225–1231, 2011.
- QIN, C. Optimization of cable-stretching planning in the construction of cable-stayed bridges. *Engineering optimization*, Taylor & Francis, v. 19, n. 1, p. 1–20, 1992.
- RAHAMI, H.; KAVEH, A.; GHOLIPOUR, Y. Sizing, geometry and topology optimization of trusses via force method and genetic algorithm. *Engineering Structures*, Elsevier, v. 30, n. 9, p. 2360–2369, 2008.



- ROJAS, I.; GONZÁLEZ, J.; POMARES, H.; MERELO, J.; CASTILLO, P.; ROMERO, G. Statistical analysis of the main parameters involved in the design of a genetic algorithm. *Systems, Man, and Cybernetics, Part C: Applications and Reviews, IEEE Transactions on, IEEE*, v. 32, n. 1, p. 31–37, 2002.
- RÜSCH, H. *Berechnungstabeln für rechtwinklige Fahrbahnplatten von Straßenbrücken*. [S.l.]: Ernst, 1965.
- SCHERVISH, M. J. *Theory of statistics*. [S.l.]: Springer Science & Business Media, 2012.
- SHARAFI, P.; TEH, L. H.; HADI, M. N. Shape optimization of thin-walled steel sections using graph theory and aco algorithm. *Journal of Constructional Steel Research*, Elsevier, v. 101, p. 331–341, 2014.
- SHEA, K.; SMITH, I. F. Improving full-scale transmission tower design through topology and shape optimization. *Journal of structural engineering*, American Society of Civil Engineers, v. 132, n. 5, p. 781–790, 2006.
- SOUZA, R. R.; MIGUEL, L. F. F.; LOPEZ, R. H.; MIGUEL, L. F. F.; TORII, A. J. A procedure for the size, shape and topology optimization of transmission line tower structures. *Engineering Structures*, Elsevier, X, n. X, p. X–X, 2015.
- STUCCHI, F. R. *Pontes e Grandes Estruturas*. [S.l.]: Escola Politécnica, Universidade de São Paulo, 2006.
- TANG, W.; TONG, L.; GU, Y. Improved genetic algorithm for design optimization of truss structures with sizing, shape and topology variables. *International Journal for Numerical Methods in Engineering*, Wiley Online Library, v. 62, n. 13, p. 1737–1762, 2005.
- TANIWAKI, K.; OHKUBO, S. Optimal synthesis method for transmission tower truss structures subjected to static and seismic loads. *Structural and Multidisciplinary Optimization*, Springer, v. 26, n. 6, p. 441–454, 2004.
- TOMA, S.; DUAN, L.; CHEN, W. F. Bridge structures. In: \_\_\_\_\_. *Structural Engineering Handbook Ed.* [S.l.: s.n.], 1999.
- TORII, A. J.; LOPEZ, R. H.; BIONDINI, F. An approach to reliability-based shape and topology optimization of truss structures. *Engineering Optimization*, Taylor & Francis, v. 44, n. 1, p. 37–53, 2012.

- TORII, A. J.; LOPEZ, R. H.; MIGUEL, L. F. Modeling of global and local stability in optimization of truss-like structures using frame elements. *Structural and Multidisciplinary Optimization*, Springer, p. 1–12, 2014.
- VANDERPLAATS, G. Structural design optimization status and direction. *Journal of Aircraft*, v. 36, n. 1, p. 11–20, 1999.
- VAZ, L. E. Método dos elementos finitos em análise de estruturas. *Campus*, 2011.
- VITÓRIO, J. A. P. Pontes metálicas e mistas tópicos de conservação, danos e reforços estruturais. 2015.
- WANG, H.; OHMORI, H. Elasto-plastic analysis based truss optimization using genetic algorithm. *Engineering Structures*, Elsevier, v. 50, p. 1–12, 2013.
- WHITLEY, D.; BEVERIDGE, R.; GRAVES, C.; MATHIAS, K. Test driving three 1995 genetic algorithms: new test functions and geometric matching. *Journal of Heuristics*, Springer, v. 1, n. 1, p. 77–104, 1995.
- WOLPERT, D. H.; MACREADY, W. G. No free lunch theorems for optimization. *Evolutionary Computation, IEEE Transactions on, IEEE*, v. 1, n. 1, p. 67–82, 1997.
- YANG, R. Multidiscipline topology optimization. *Computers & Structures*, Elsevier, v. 63, n. 6, p. 1205–1212, 1997.
- YANG, X.-S. Firefly algorithm. *Engineering Optimization*, Wiley Online Library, p. 221–230, 2010.
- ZHOU, H.; SHI, G.; WANG, Y.; CHEN, H.; ROECK, G. D. Fatigue evaluation of a composite railway bridge based on fracture mechanics through global–local dynamic analysis. *Journal of Constructional Steel Research*, Elsevier, v. 122, p. 1–13, 2016.

# Annex



## **Annex A**

### **Rüsch's tables**





#			Uniform distributed load in the plate For $M_{xe}$ $k = -0.50$ For $M_{yr}$ $k = 0$		$M = k \times g \times l_x^2$ g or p in t/m <sup>2</sup> ; $l_x$ in m				
	Bridge Class from 30 t to 60 t		Tire load of 1,0 t		Uniform distributed load of 1 t/m <sup>2</sup>				
$l_x/a$	- $M_{xe}$ in the middle of the edge t/a		- $M_{yr}$ in the middle of the free edge t/a		For all values of t/a				
	L	L	L	L	p	p'			
0.125	0.250	0.500	1.000	0.125	0.250	0.500	1.000		
0.125	0.110	0.100	0.040	0.170	0.100	0.060	0.010	-	p'
0.250	0.230	0.200	0.100	0.270	0.180	0.100	0.012	-	-
0.375	0.330	0.330	0.180	0.340	0.230	0.125	0.020	-	-
0.500	0.520	0.510	0.280	0.390	0.265	0.145	0.040	-	-
0.625	0.700	0.670	0.433	0.425	0.287	0.160	0.052	-	-
0.750	0.900	0.870	0.630	0.440	0.300	0.160	0.080	-	-
1.000	1.240	1.180	0.950	0.500	0.360	0.220	0.135	0.05	-
1.250	1.500	1.440	1.340	0.580	0.448	0.309	0.216	0.23	-
1.500	1.720	1.660	1.570	0.680	0.540	0.422	0.310	0.38	0.04
1.750	1.900	1.850	1.760	0.790	0.660	0.550	0.415	0.70	0.06
2.000	2.040	2.000	1.930	0.910	0.780	0.690	0.530	1.24	0.08
2.250	2.180	2.150	2.100	1.040	0.910	0.840	0.650	1.98	0.10
2.500	2.290	2.290	2.230	1.170	1.040	0.900	0.770	3.24	0.15

Figure 37 – Rüsç's table 98 - part 1



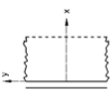
#			Uniform distributed load in the plate															
	$I_y / I_x = \infty$		$M = k \times g \times l_x^2$															
	For $M_{ym}$ $k = 0$		For $M_{xm}$ $k = -0,125$															
		g or p in t/m <sup>2</sup> ; k in m																
98	Bridge Class from 30 t to 60 t				Tire load of 1,0 t				Uniform distributed load of 1 t/m <sup>2</sup>									
	$+ M_{ym}$ in the middle of the plate		$+ M_{ym}$ in the middle of the plate		$- M_{xm}$ in the middle of the plate		$- M_{xm}$ in the middle of the plate		$+ M_{ym}$		$+ M_{ym}$		$- M_{xm}$					
$l_x / a$	t / a				t / a				For all values of t/a									
	0.125	0.250	0.500	1.000	0.125	0.250	0.500	1.000	0.125	0.250	0.500	1.000	p	p'	p	p'	p	p'
0.125	L	L	L	L	L	L	L	L	L	L	L	L	-	-	-	-	-	-
0.175	0.046	0.013	0.007	0.001	0.075	0.048	0.014	0.003	0.056	0.043	0.013	0.010	-	-	-	-	-	-
0.250	0.074	0.024	0.015	0.001	0.100	0.068	0.027	0.005	0.100	0.086	0.056	0.024	-	-	-	-	-	-
0.375	0.092	0.035	0.020	0.001	0.118	0.082	0.036	0.007	0.136	0.130	0.090	0.040	-	-	-	-	-	-
0.500	0.102	0.048	0.027	0.002	0.131	0.091	0.046	0.010	0.176	0.174	0.124	0.060	-	-	-	-	-	-
0.625	0.110	0.061	0.033	0.003	0.142	0.097	0.052	0.017	0.218	0.218	0.154	0.079	-	-	-	-	-	-
0.750	0.114	0.075	0.038	0.012	0.156	0.103	0.060	0.034	0.266	0.263	0.200	0.104	-	-	-	-	-	-
1.000	0.124	0.094	0.051	0.026	0.180	0.125	0.085	0.062	0.330	0.328	0.263	0.150	-	-	-	-	-	-
1.250	0.133	0.110	0.065	0.040	0.195	0.142	0.118	0.093	0.377	0.373	0.313	0.196	-	-	-	-	-	-
1.500	0.155	0.133	0.092	0.062	0.240	0.185	0.169	0.133	0.414	0.410	0.354	0.239	-	-	-	-	-	-
1.750	0.179	0.158	0.121	0.084	0.285	0.225	0.225	0.175	0.444	0.442	0.390	0.280	-	-	-	-	-	-
2.000	0.203	0.185	0.154	0.109	0.350	0.322	0.290	0.212	0.470	0.468	0.420	0.318	-	-	-	-	-	-
2.250	0.240	0.214	0.189	0.133	0.428	0.405	0.356	0.250	0.490	0.487	0.447	0.356	-	-	-	-	-	-
2.500	0.274	0.245	0.225	0.158	0.510	0.500	0.430	0.285	0.510	0.510	0.471	0.391	-	-	-	-	-	-

Figure 38 – Rüsç’s table 98 - part 2